

# 1 **Reconstruction of Solar Extreme Ultraviolet Flux 1740–2015**

2  
3 Leif Svalgaard<sup>1</sup> ([leif@leif.org](mailto:leif@leif.org))

4 <sup>1</sup> Stanford University, Cypress Hall C13, W.W. Hansen Experimental Physics  
5 Laboratory, Stanford University, Stanford, CA 94305, USA

## 6 7 **Abstract:**

8 Solar Extreme Ultraviolet (EUV) radiation creates the conducting E-layer of the  
9 ionosphere, mainly by photo ionization of molecular Oxygen. Solar heating of the  
10 ionosphere creates thermal winds which by dynamo action induce an electric field driving  
11 an electric current having a magnetic effect observable on the ground, as was discovered  
12 by G. Graham in 1722. The current rises and sets with the Sun and thus causes a readily  
13 observable diurnal variation of the geomagnetic field, allowing us to deduce the  
14 conductivity and thus the EUV flux as far back as reliable magnetic data reach. High-  
15 quality data go back to the ‘Magnetic Crusade’ of the 1830s and less reliable, but still  
16 usable, data are available for portions of the hundred years before that. J.R. Wolf and,  
17 independently, J.-A. Gautier discovered the dependence of the diurnal variation on solar  
18 activity, and today we understand and can invert that relationship to construct a reliable  
19 record of the EUV flux from the geomagnetic record. We compare that to the F10.7 flux  
20 and the sunspot number, and find that the reconstructed EUV flux reproduces the F10.7  
21 flux with great accuracy. On the other hand, it appears that the Relative Sunspot Number  
22 as currently defined is beginning to no longer be a faithful representation of solar  
23 magnetic activity, at least as measured by the EUV and related indices. The  
24 reconstruction suggests that the EUV flux reaches the same low (but non-zero) value at  
25 every sunspot minimum (possibly including Grand Minima), representing an invariant  
26 ‘solar magnetic ground state’.

27  
28 **Keywords:** Solar EUV flux; Geomagnetic diurnal variation; Ionospheric E-layer; Long-  
29 term variation of solar activity

30

## 31 1. Introduction

32 Graham (1724) discovered that the Declination, i.e. the angle between the horizontal  
33 component of the geomagnetic field (as shown by a compass needle) and true north,  
34 varied through the day. Canton (1759) showed that the range of the daily variation varied  
35 with the season, being largest in summer. Lamont (1851) noted that the range had a clear  
36 ~10–year variation, whose amplitude Wolf (1852a, 1857) and Gautier (1852) found to  
37 follow the number of sunspots varying in a cyclic manner discovered by Schwabe (1844).  
38 Thus was found a relationship between the diurnal variation and the sunspots “not only in  
39 average period, but also in deviations and irregularities” establishing a firm link between  
40 solar and terrestrial phenomena and opening up a whole new field of science. This was  
41 realized immediately by both Wolf and Gautier and recognized by many distinguished  
42 scientists of the day. Faraday wrote to Wolf on 27th August, 1852 (Wolf, 1852b):

43 *I am greatly obliged and delighted by your kindness in speaking to me of your most*  
44 *remarkable enquiry, regarding the relation existing between the condition of the*  
45 *Sun and the condition of the Earths magnetism. The discovery of periods and the*  
46 *observation of their accordance in different parts of the great system, of which we*  
47 *make a portion, seem to be one of the most promising methods of touching the*  
48 *great subject of terrestrial magnetism...*

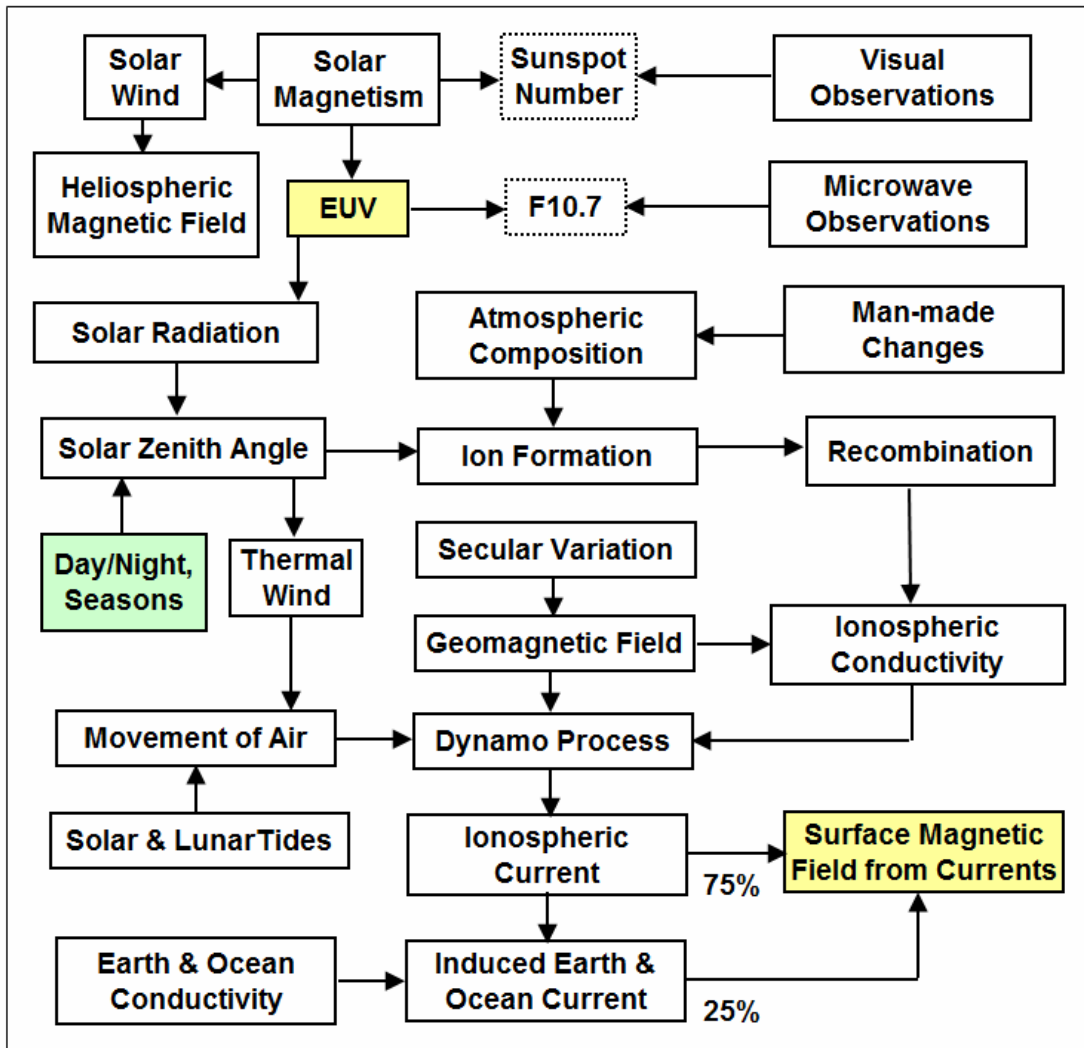
49 Wolf soon found (Wolf, 1859) that there was a simple, linear relationship between the  
50 yearly average amplitude,  $v$ , of the diurnal variation of the Declination and his relative  
51 sunspot number,  $R$ :  $v = a + bR$  with coefficients  $a$  and  $b$ , allowing him to calculate the  
52 terrestrial response from his sunspot number, determining  $a$  and  $b$  by least squares. He  
53 marveled “Who would have thought just a few years ago about the possibility of  
54 computing a terrestrial phenomenon from observations of sunspots”.

55 Later researchers, (e.g. Chree, 1913; Chapman *et al.*, 1971), wrote the relationship in the  
56 equivalent form  $v = a(1 + mR/10^4)$  separating out the solar modulation in the  
57 unit-independent parameter  $m$  (avoiding decimals using the device of multiplying by  $10^4$ )  
58 with, it was hoped, local influences being parameterized by the coefficient  $a$ . Chree also  
59 established that  $a$  and  $m$  for a given station (geomagnetic observatory) were the same on  
60 geomagnetically quiet and geomagnetic disturbed days, showing that another relationship  
61 found with magnetic disturbances (Sabine, 1852) hinted at a different nature of *that*  
62 solar–terrestrial relation; a difference that for a long time was not understood and that  
63 complicates analysis of the older data (Macmillan and Droujinina, 2007).

64 Stewart (1882) suggested that the diurnal variation was due to the magnetic effect of  
65 electric currents flowing in the high atmosphere, such currents arising from electromotive  
66 forces generated by periodic (daily) movements of an electrically conducting layer across  
67 the Earth’s permanent magnetic field. The next step was taken independently by  
68 Kennelly (1902) and Heaviside (1902) who pointed out that if the upper atmosphere was  
69 electrically conducting it could guide radio waves round the curvature of the Earth thus  
70 explaining the successful radio communication between England and Newfoundland  
71 established by Marconi in 1901. It would take another three decades before the notion of  
72 conducting ionospheric layers was clearly understood and accepted (Appleton, Nobel  
73 Lecture, 1947): the E–layer electron density and conductivity start to increase at sunrise,

74 reach a maximum near noon, and then wane as the Sun sets; the variation of the  
 75 conductivity through the sunspot cycle being of the magnitude required to account for the  
 76 change with the sunspot number of the magnetic effects measured on the ground.

77 The Solar Extreme Ultraviolet (EUV) radiation causes the observed variation of the  
 78 geomagnetic field at the surface through a complex chain of physical connections (as first  
 79 suggested by Schuster (1908)), see Figure 1. The physics of most of the links of the chain  
 80 is reasonably well-understood in quantitative detail and can often be successfully  
 81 modeled. We shall use this chain *in reverse* to deduce the EUV flux from the  
 82 geomagnetic variations, touching upon several interdisciplinary subjects.



113 Figure 1: Block diagram of the entities and processes causally connecting variation of the solar magnetic field to the regular diurnal variation of the geomagnetic field.  
 114 The effective ionospheric conductivity is a balance between ion formation and  
 115 recombination. The movement of electrons across the geomagnetic field drives an  
 116 efficient dynamo providing the electromotive force for the ionospheric currents  
 117 giving rise to the observed diurnal variations of the geomagnetic field. The various  
 118 blocks are further described in the text below.  
 119

120 Solar magnetism (as directly observed and as derived from its proxy, the sunspot number)  
 121 gives rise to an (observable) Extreme Ultraviolet (EUV) excess over that expected from  
 122 solar blackbody radiation and also ultimately heats the corona to drive an (observable)  
 123 solar wind with an embedded (and observable) heliospheric magnetic field. The  
 124 (observable) F10.7 microwave flux is generally thought to be a good proxy for the EUV  
 125 flux. Solar radiation onto the atmosphere is controlled by the solar zenith angle and  
 126 causes thermal winds which, in combination with solar (and lunar) tides, move air across  
 127 geomagnetic field lines. Radiation with a short-enough wave length ionizes atmospheric  
 128 constituents (primarily molecular Oxygen), and there is a balance between the ion  
 129 formation and subsequent rapid recombination establishing an (observable) ionospheric  
 130 conducting layer of electrons and ions that due to collisions moves with the winds of the  
 131 neutral air across the (observable) geomagnetic field. The resulting inductive dynamo  
 132 maintains an electric current whose magnetic effect is observable on the ground. The day-  
 133 night cycle imposes an (observable) diurnal variation of the magnetic effect which has  
 134 been observed for several centuries. The varying magnetic field induces additional (but  
 135 smaller) currents underground and in the oceans. The output of the entire process is the  
 136 (observable) total daily range of the magnetic variation that can be readily observed over  
 137 a wide range of latitude. In the following sections we describe the salient physics in more  
 138 detail.

## 139 2. The Ionospheric E–Layer

140 The dynamo process takes place in the dayside E–layer where the density, both of the  
 141 neutral atmosphere and of electrons is high enough. The conductivity at a given height is  
 142 roughly proportional to the electron number density  $N_e$ . In the dynamo region (at 105 km  
 143 altitude), the dominant plasma species is molecular oxygen ions,  $O_2^+$ , produced by photo  
 144 ionization (by photons of wavelength  $\lambda$  of 102.7 nm or less (Samson and Gardner, 1975))  
 145 at a rate  $J$  per unit time  $O_2 + h\nu \xrightarrow{J} O_2^+ + e^-$  and lost through recombination with  
 146 electrons at a rate  $\alpha$  per unit time  $O_2^+ + e^- \xrightarrow{\alpha} O + O$ , in the process producing the  
 147 Airglow. The rate of change of the number of ions,  $N_i$ ,  $dN_i/dt$  and of electrons,  $N_e$ ,  $dN_e/dt$   
 148 are given by  $dN_i/dt = J \cos(\chi) - \alpha N_i N_e$  and  $dN_e/dt = J \cos(\chi) - \alpha N_e N_i$ , respectively,  
 149 where we have ignored motions into or out of the layer. Since the Zenith angle  $\chi$  changes  
 150 but slowly, we have a quasi steady–state (with a time constant of order  $1/(2\alpha N) \approx 1$   
 151 minute), in which there is no net electric charge, so  $N_i = N_e = N$ . In steady state  $dN/dt = 0$ ,  
 152 so that the equations can both be written  $0 = J \cos(\chi) - \alpha N^2$ , or when solving for the  
 153 number of electrons  $N = \sqrt{J \cos(\chi) / \alpha}$  (using the sufficient approximation of a flat Earth  
 154 with a layer of uniform density). Since the conductivity,  $\Sigma$ , depends on the number of  
 155 electrons we expect that  $\Sigma$  should scale with the square root  $\sqrt{J}$  of the overhead EUV  
 156 flux (Yamazaki and Kosch, 2014). Even if the exponent is not quite  $1/2$  (e.g. Ieda *et al.*,  
 157 2014), that is not critical to and has no influence on the result of our analysis.

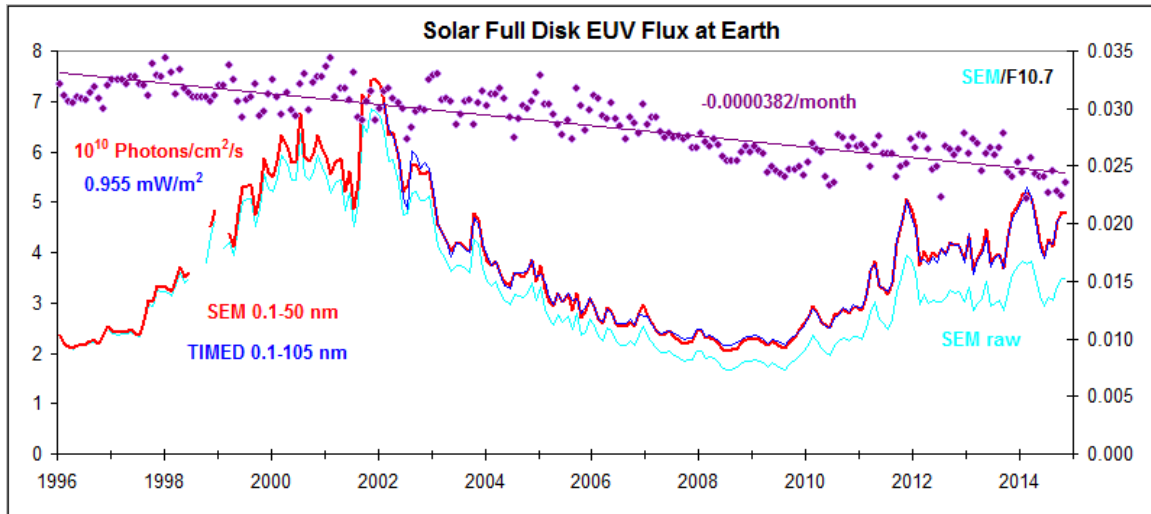
158 The magnitude,  $A$ , of the variation of the East Component due to the dynamo process is  
 159 given by  $A = \mu_0 \Sigma U B_z$  (Takeda, 2013) where  $\mu_0$  is the permeability of the vacuum  
 160 ( $4\pi \times 10^{-7}$ ),  $\Sigma$  is the height–integrated effective ionospheric conductivity (in S),  $U$  is the  
 161 zonal neutral wind speed (m/s), and  $B_z$  is the vertical geomagnetic field strength (nT).  
 162 The conductivity is a highly anisotropic tensor and in the E–layer the electrons begin to  
 163 gyrate and drift perpendicular to the electric field, while the ions still move in direction of

164 the electric field; the difference in direction is the basis for the Hall conductivity  $\Sigma_H$ ,  
165 which is there larger than the Pedersen conductivity  $\Sigma_P$ . The combined conductivity then  
166 becomes  $\Sigma = \Sigma_P + \Sigma_H^2/\Sigma_P$  (Koyama *et al.*, 2014; Ieda *et al.*, 2014; Takeda, 2013; Maeda,  
167 1977).

168 The various conductivities depend on the ratio between the electron density  $N$  and the  
169 geomagnetic field  $B$  times a slowly varying dimensionless function involving ratios of  
170 gyro frequencies  $\omega$  and collision frequencies  $\nu$ :  $N/B \times f(\omega_e, \nu_{en\perp}, \omega_i, \nu_{in})$  (Richmond, 1995)  
171 such that, to first approximation,  $\Sigma \sim N/B$  (Clilverd *et al.*, 1998), with the result that the  
172 magnitude  $A$  only depends on the electron density and the zonal neutral wind speed. On  
173 the other hand, simulations by Cnossen *et al.* (2012) indicate a stronger dependence on  $B$   
174 (actually on the nearly equivalent magnetic dipole moment of the geomagnetic field  $M$ ),  
175  $\Sigma \propto M^{-1.5}$ , leading to a dependence of  $A$  on  $M$ :  $A \propto M^{-0.85}$ , and thus expected to cause a  
176 small secular increase of  $A$  as  $M$  is decreasing over time This stronger dependence is  
177 barely, if at all, seen in the data. We return to this point in Section 7. The purported near-  
178 cancellation of  $B$  is not perfect, though, depending on the precise geometry of the field. In  
179 addition, the ratio between internal and external current intensity varies with location.  
180 The net result is that  $A$  can and does vary somewhat from location to location even for  
181 given  $N$  and  $U$ . Thus a normalization of the response to a reference location is necessary,  
182 as discussed in detail in Section 7.

### 183 **3. The EUV Emission Flux**

184 The Solar EUV Monitor (CELIAS/SEM) onboard the SOHO spacecraft at Lagrange  
185 Point L1 has measured the integrated solar EUV emission in the 0.1–50 nm band since  
186 1996 (Judge *et al.*, 1998). The calibrated flux (version 3) at a constant solar distance of 1  
187 AU is from [http://www.usc.edu/dept/space\\_science/semdatafolder/long/daily\\_avg/](http://www.usc.edu/dept/space_science/semdatafolder/long/daily_avg/). For  
188 our purpose, we reduce all flux values to the Earth’s distance and compute monthly  
189 averages. The main degradation of the SEM sensitivity is attributed to build-up (and  
190 subsequent polymerization by UV photons) of a hydrocarbon contaminant layer on the  
191 entrance filter, and is mostly corrected for using a model of the contaminant deposition.  
192 We estimate any *residual* degradation by monitoring the ratio between the reported SEM  
193 EUV flux (turquoise curve in Figure 2) and the F10.7 microwave flux, Figure 2 (purple  
194 points), and adjusting the SEM flux accordingly (red curve). The issue of degradation of  
195 SEM has been controversial (Lean *et al.*, 2011; Emmert *et al.*, 2014; Didkovsky and  
196 Wieman, 2014) and is, perhaps, still not completely resolved (Wieman *et al.*, 2014). We  
197 constrain the SEM flux to match F10.7 as suggested by Emmert *et al.* (2014).  
198



199  
200  
201  
202  
203  
204  
205  
206  
207

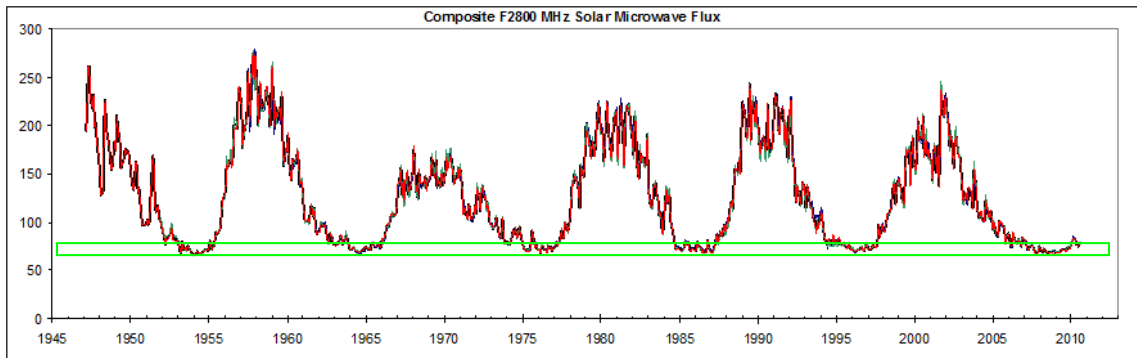
Figure 2: Integrated CELIAS–SEM absolute solar EUV flux in the 0.1–50 nm band (turquoise curve) uncorrected for *residual* degradation of the instrument and the corrected flux (red curve) as derived from the decrease of the ratio between the raw EUV flux and the F10.7 microwave flux (purple points). The degradation–corrected integrated flux in the 0.1–105 nm band measured by TIMED (blue curve) matches the corrected SEM flux requiring only a simple, constant scaling factor. All data are as measured at Earth rather than at 1 AU.

208 The Solar EUV Experiment (SEE) data from the NASA ‘Thermosphere, Ionosphere,  
209 Mesosphere Energetics and Dynamics (TIMED)’ mission (Woods *et al.*, 2005) provide,  
210 since 2002, daily averaged solar irradiance in the 0.1–105 nm band with corrections  
211 applied for degradation and atmospheric absorption (version 11 with flare spikes  
212 removed) and can be downloaded from <http://lasp.colorado.edu/home/see/data/>. The SEE  
213 flux (Figure 2, blue curve) is very strongly linearly correlated with (and simply  
214 proportional to) our residual–degradation–corrected SEM flux (with coefficient of  
215 determination  $R^2 = 0.99$ ) and thus serves as validation of the corrected SEM data. SEM  
216 data is in units of photons/cm<sup>2</sup>/s while SEE data is in units of mW/m<sup>2</sup>. Using the SEE  
217 reference spectrum in bins of 1 nm integrated from 0 to 50 nm, the two scales can be  
218 converted to each other ( $10^{10}$  photons/cm<sup>2</sup>/s ↔ 0.955 mW/m<sup>2</sup>). We shall here use a  
219 composite of the SEM and SEE data in SEM units. All data used are supplied in the  
220 Supplementary Data Section of this paper.

#### 221 4. The F10.7 Flux Density

222 The  $\lambda$ 10.7 cm microwave flux (F10.7) has been routinely measured in Canada (first at  
223 Ottawa and then at Penticton) since 1947 and is an excellent indicator of the amount of  
224 magnetic activity on the Sun (Tapping, 1987, 2013). The 10.7 cm wavelength  
225 corresponds to the frequency 2800 MHz. Measurements of the microwave flux at several  
226 frequencies from 1000 MHz ( $\lambda$ 30 cm) to 9400 MHz ( $\lambda$ 3.2 cm), straddling 2800 MHz,  
227 have been carried out in Japan (first at Toyokawa and then at Nobeyama) since the 1950s  
228 (Shibasaki *et al.*, 1979) and allow a cross–calibration with the Canadian data. A 2%  
229 decrease of the 2800 MHz flux is indicated when the Canadian radiometer was moved

230 from Ottawa to Penticton in mid–1991 (Svalgaard, 2010). We correct for this by reducing  
 231 the Ottawa flux accordingly. As the morning and afternoon measurements at Penticton  
 232 are, at times (especially during the snowy winter), afflicted with systematic errors (of  
 233 unknown provenance) we only use the noon–values of the observed flux (not adjusted to  
 234 a solar distance of 1 AU) and form a composite (updated through 2014) with the Japanese  
 235 data (for 2000 and 3750 MHz) scaled to the Canadian 2800 MHz (Svalgaard, 2010;  
 236 Svalgaard and Hudson, 2010), Figure 3, similar to the composite by Dudok de Wit *et al.*  
 237 (2013).



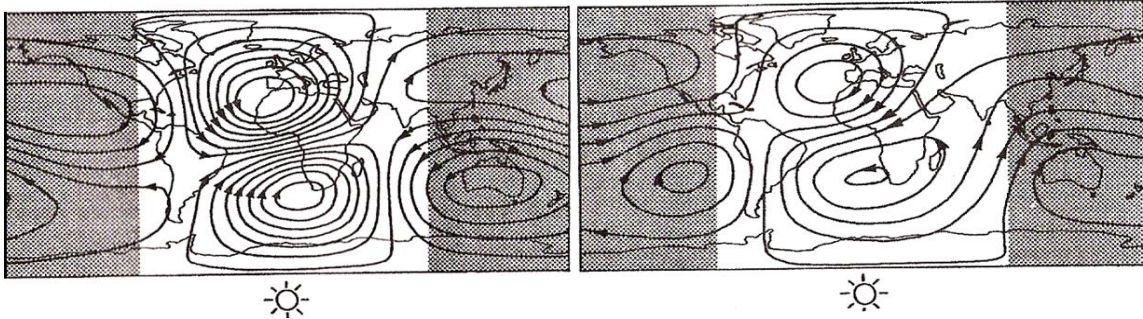
238

239 Figure 3: Composite 2800 MHz solar microwave flux (thin black curve) built from  
 240 Canadian 2800 MHz flux (red curve), scaled Japanese 3750 MHz flux (green  
 241 curve), and scaled Japanese 2000 MHz flux (blue curve), Svalgaard (2010). The  
 242 match is so good that it is difficult to see the individual curves as they fall on top of  
 243 each other. Note that the values at each sunspot minimum are very similar, without  
 244 any long-term trend or inter-cycle variation.

245 The reported F10.7 data can be downloaded from the Dominion Radio Astrophysical  
 246 Observatory at [ftp://ftp.geolab.nrcan.gc.ca/data/solar\\_flux/daily\\_flux\\_values/](ftp://ftp.geolab.nrcan.gc.ca/data/solar_flux/daily_flux_values/). Although  
 247 the absolute calibration of the observed flux density shows that the flux values must be  
 248 multiplied by 0.9 (the ‘URSI’ adjustment), we follow tradition and do not apply this  
 249 adjustment. The Japanese data can be downloaded from <http://solar.nro.nao.ac.jp/norp/>.

## 250 5. The $S_R$ Current System

251 More than 200 geomagnetic observatories around the world measure the variation of the  
 252 Earth’s magnetic field from which the *regular*, solar local time daily variations described  
 253 by Canton (1759) and Mayaud (1965),  $S_R$ , can be derived. From the variation of the  
 254 horizontal component  $\Delta H$ , one can derive the surface current density,  $K$ , for a  
 255 corresponding equivalent thin–sheet electric current system overhead,  $K$  (mA/m) = 1.59  
 256  $\Delta H$  (nT) =  $2\Delta H/\mu_0$ . This relationship is not unique; the current system is three–  
 257 dimensional, and an infinite number of current configurations fit the magnetic variations  
 258 observed at ground level. Measurements in space provide a much more realistic picture  
 259 (Olsen, 1996) and the  $S_R$  system is only a convenient *representation* of the true current.



260  
 261 Figure 4: Streamlines of equivalent  $S_R$  currents during equinox at 12 UT separately  
 262 for the external primary (left) and the internal secondary (right) currents (Adapted  
 263 after Malin, 1973).

264 Figure 4 (left) shows current streamlines of the equivalent  $S_R$  current as seen from the  
 265 Sun at (Greenwich) noon. This current configuration is fixed with respect to the Sun with  
 266 the Earth rotating beneath it. The westward moving  $S_R$  current vortex and the electrically  
 267 conducting Earth interior (and ocean) act as a transformer with the E-layer as the primary  
 268 winding and the conducting ground as the secondary winding, inducing electric currents  
 269 at depth. The magnetic field of the secondary current (about 30% of that of the primary)  
 270 adds to the magnetic field of the primary  $S_R$  current. We are concerned only with the total  
 271 variation resulting from superposition of the two components. In addition, we do not limit  
 272 ourselves to the variation on the so-called ‘quiet days’, as their level of quietness varies  
 273 with time, but rather use data from all days when available (the difference is in any case  
 274 small).

275 The  $S_R$  current depends on season, i.e. the solar Zenith angle controlling the flux of EUV  
 276 radiation onto the surface. The summer vortex is larger and stronger than the winter  
 277 vortex and actually spills over into the winter hemisphere. The amplitude of the  $S_R$   
 278 increases by a factor of two from solar minimum to solar maximum, mostly due to the  
 279 solar cycle variation of conductivity caused by the solar cycle variation of the EUV flux  
 280 (Lean *et al.*, 2003). In addition, the daytime vortices show a day-to-day variability,  
 281 attributed to upward-traveling internal waves that are sensitive to varying conditions in  
 282 the lower atmosphere.

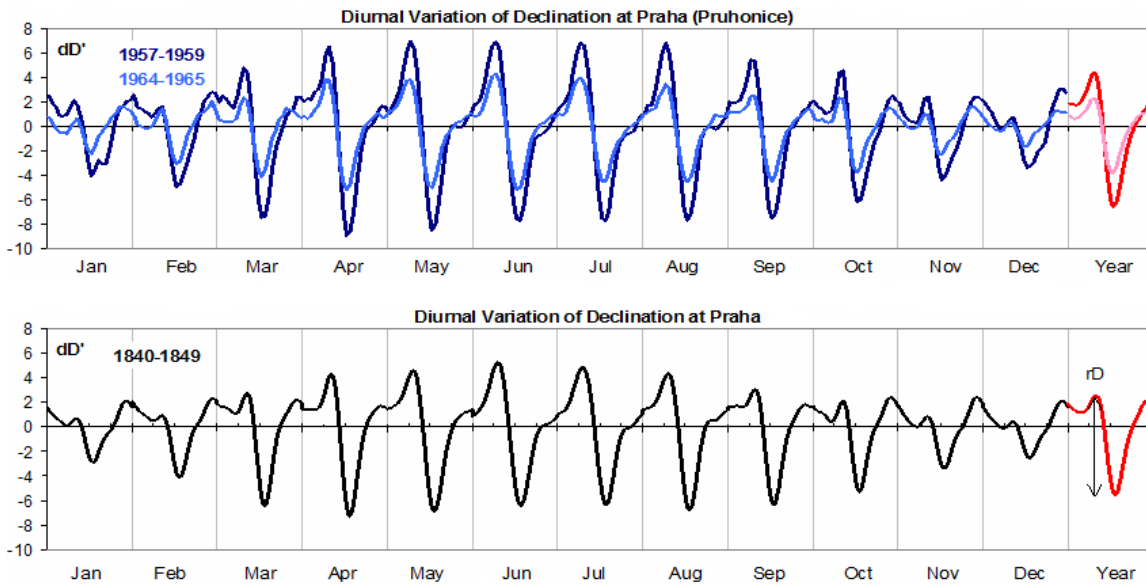
283 Atmospheric magnetic tides (Love and Rigler, 2014) are global-scale waves excited by  
 284 differential solar heating or by gravitational tidal forces of both the Moon and the Sun.  
 285 The atmosphere behaves like a large (imperfect) waveguide closed at the surface at the  
 286 bottom and open to space at the top, allowing an infinite number of atmospheric wave  
 287 modes to be excited, but only low-order modes are important. The lunar tide is ~20 times  
 288 smaller and will not be considered further here.

## 289 **6. The Diurnal Range of the Geomagnetic East Component**

290 The  $S_R$  current system rises with the Sun in the morning, with the pre-noon current at  
 291 northern mid-latitudes running from north to south (in the opposite direction at southern  
 292 latitudes) and when the Sun and the currents set, the afternoon current is from south to  
 293 north (Figure 4). The magnetic effect due to these currents is at right angles to the current  
 294 direction, i.e. east-west. Currents due to solar wind induced geomagnetic disturbances  
 295 (Ring Current; electrojets) tend to flow east-west, so their magnetic effect is strongest in



296 the north-south direction and generally lowest and rather disorganized in the east–west  
 297 direction, hence have little effect on the average east–west magnetic variations. For this  
 298 reason, the variation of the geomagnetic East–Component (and the almost equivalent  
 299 Declination, Figure 5) is especially suited as a proxy for the strength of the  $S_R$  current.



300  
 301 Figure 5: Diurnal variation of Declination (in arc minutes) at Prague per month. For  
 302 each month is shown the variation (with respect to the daily mean) over one local  
 303 solar day from midnight through noon to the following midnight. Top: modern data  
 304 for low sunspot number (1964–1965, light blue) and for high sunspot number  
 305 (1957–1959, dark blue). Bottom: average for the interval 1840–1849. The red  
 306 curves show the yearly averages. The range,  $rD$ , should be defined as the difference  
 307 between the values of the pre-noon and post-noon local extrema, rather than  
 308 simply between the highest and lowest values for day.

309 Some geomagnetic observatories report measurements of the Horizontal Component  $H$   
 310 and the Declination  $D$ , while others report the North and East Components,  $X$  and  $Y$ ,  
 311 determined by  $X = H \cos(D)$ ,  $Y = H \sin(D)$ . For a small change  $dD'$  (arc minutes) in  $D$ ,  
 312 the change in  $Y$  is often approximated by  $dY = H \cos(D) dD'/3438'$ . We convert all  
 313 variations directly to force units (nT) without using the approximation, whenever  
 314 possible. Many early observers did not measure  $H$ , but only  $D$ . We can still calculate  $Y$   
 315 because  $H$  can with sufficient accuracy as needed be determined for any location from  
 316 historical spherical harmonics coefficients at any time in the past 400 years (Jackson *et*  
 317 *al.*, 2000). Actually, there is a benefit to using the angle  $D$ , as angles do not need  
 318 calibration. It is clear from Figure 5 that the measurements from the 1840s are accurate  
 319 enough to show, even in minute detail, the same variations as the modern data and that  
 320 the amplitude, and hence solar activity, back then was intermediate between that in 1964–  
 321 1965 and 1957–1959.

322 In order to construct a long–term record we shall work with yearly averages of the range,  
 323  $rY$ , of the diurnal variation of the East–Component, defined as the unsigned difference  
 324 between the values of the pre-noon and post-noon local extrema of  $Y$ . The values can be  
 325 hourly averages or spot–values, the (small) difference corrected for by suitable

326 normalization, if needed. Many older stations only observed a few times a day or twice,  
327 usually near the times of maximum excursions from the mean. As long as these  
328 observations were made at fixed times during the day, they can be used to construct a  
329 nominal daily range. Most long-running observatories had to be moved to replacement  
330 stations further and further away from their original locations due to electrical and urban  
331 disturbances, forming a station ‘chain’. We usually normalize the data separately for  
332 replacement stations, except when they are co-located upgrades of the original station.

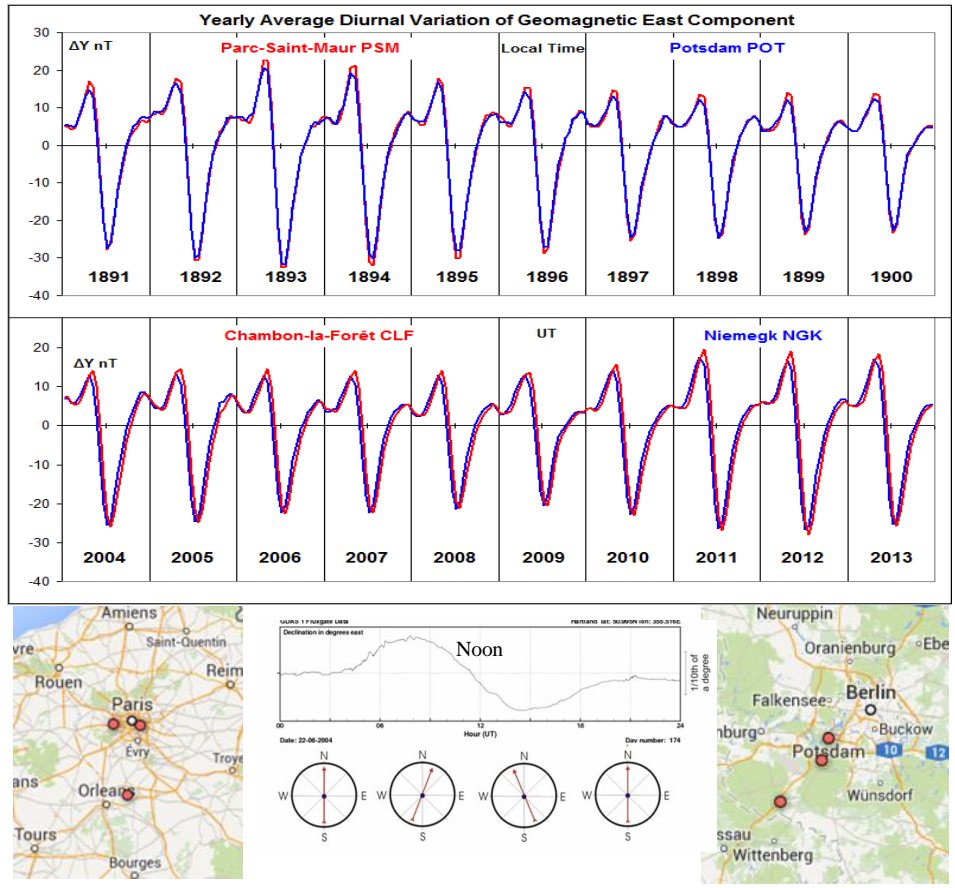
333 At mid-latitude stations (say around  $35^\circ$  latitude) the electric currents flow generally  
334 North-South over a relatively large range of latitudes, so most of the magnetic effect of  
335 the current will be in the East-West component. The magnetic effects of the auroral zone  
336 and equatorial electrojets as well as of the Ring Current are mostly in the North-South  
337 direction so are minimized by limiting our investigation to the East-component.

338 Another advantage of using the East component is that (at least generally before the 20<sup>th</sup>  
339 century) it often is based on observations of the Declination, which, being an angle does  
340 not require calibration (other than the trivial conversion from scale values) nor difficult  
341 temperature corrections. That said, the Declination *is* sensitive to the disturbing effects of  
342 nearby iron masses. A valid criticism of the use of the range in Declination,  $rD$ , is that it  
343 is the resultant of the pull of two force vectors: the (nearly constant) largely North-South  
344 horizontal force of the main geomagnetic field and the (varying during the day) largely  
345 East-West force of the magnetic effect of the  $S_R$  current system, and that therefore the  
346 range of the angle in arc minutes varies with the horizontal force as well, in space and in  
347 time. François Arago wonderfully described (in the 1820s) how the range of the  
348 Declination he observed at the Paris Observatory increased by a factor of ten as the result  
349 of installation (later removed) of an iron stove in an adjoining room, the magnetic stove  
350 canceling out a large part of the natural horizontal force.

### 351 **6.1. The Master Record**

352 The German station chain (POT–SED–NGK) yields an almost unbroken data series  
353 extending over 125 years. The French station chain (PSM–VLJ–CLF) provides an even  
354 longer series, 130 years of high-quality data, (Fouassier and Chulliat, 2009). The diurnal  
355 variation of  $\Delta Y$  (Figure 6) is essentially the same for both chains at both ends of the  
356 series. There is a clear 0.7 hour shift of CLF with respect to NGK due to modern daily  
357 records covering a UT-day rather than the local solar day. This has negligible impact on  
358 the range  $rY$ .  
359

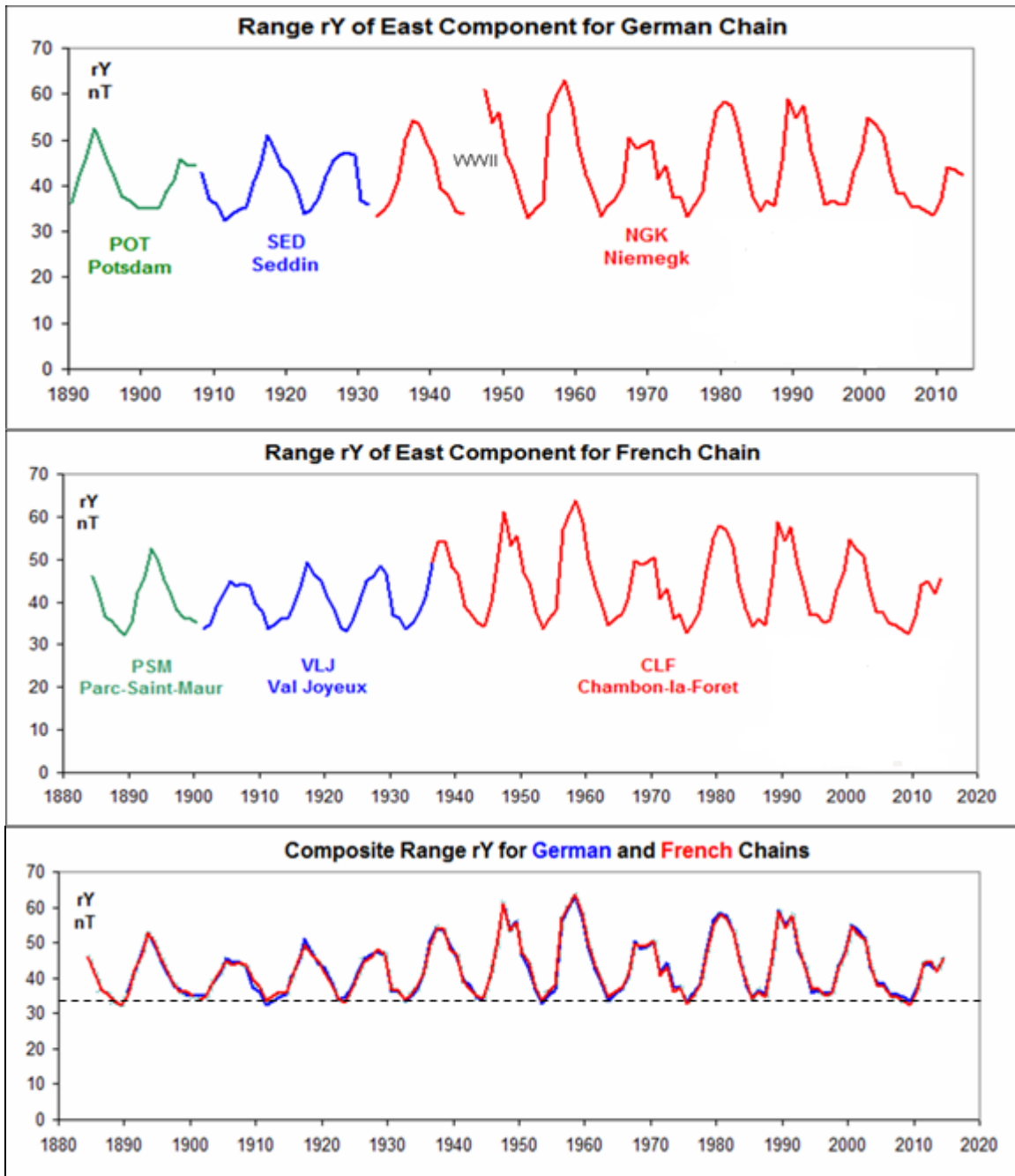
360  
 361  
 362  
 363  
 364  
 365  
 366  
 367  
 368  
 369  
 370  
 371  
 372  
 373  
 374  
 375  
 376  
 377  
 378  
 379  
 380  
 381  
 382  
 383  
 384  
 385



386 Figure 6: Yearly average diurnal variation,  $\Delta Y$ , of the East-Component for (top)  
 387 observatories PSM (France) and POT (Germany) for each year of the decade 1891–  
 388 1900, and for (center) observatories CLF (France) and NGK (Germany) for the  
 389 decade 2004–2013. (Bottom) Observatory locations and schematic variation of the  
 390 direction of the ‘magnetic needle’.

391 The variation at the French stations is 5% larger than at the German stations. We form a  
 392 simple composite Master-Record, adjusting the French stations down by 5%, Figure 7.  
 393 The Master-Record is thus fundamentally and arbitrarily rooted in the German series. No  
 394 further adjustments of the intra-chain records can be made (and none seems necessary),  
 395 as the available data for individual stations in each chain do not overlap enough in time.

396 It is immediately apparent that there is very little, if any, variation of the range at sunspot  
 397 minima (dashed line in lower panel of Figure 7). The lack of a trend in the mid-latitude  
 398 geomagnetic response to solar activity in general has also been noted by Martini *et al.*  
 399 (2015).



400

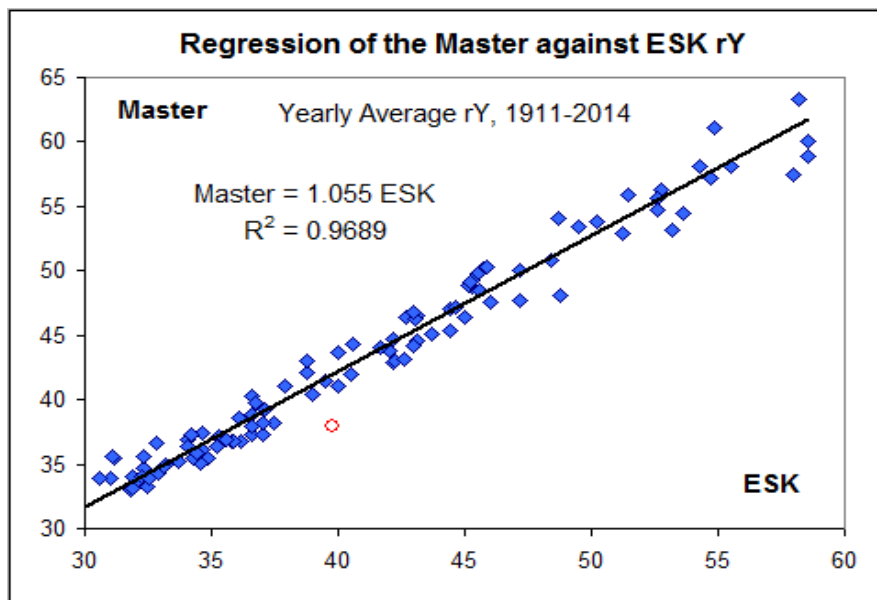
401 Figure 7: Yearly average diurnal range,  $rY$ , of the East-Component for German  
 402 stations near Berlin (top panel), for French stations near Paris (middle panel), and a  
 403 composite (bottom panel) being simply the average of the German records and of  
 404 the (scaled down by 5%) French records.

## 405 7. Normalization of the Diurnal Range, $rY$

406 The composite shall serve as a *Master-Record* to which all other stations will be  
 407 normalized. The vertical component in Central Europe over the time period of the  
 408 *Master-Record* has increased by some 3%. We would expect a corresponding 2%

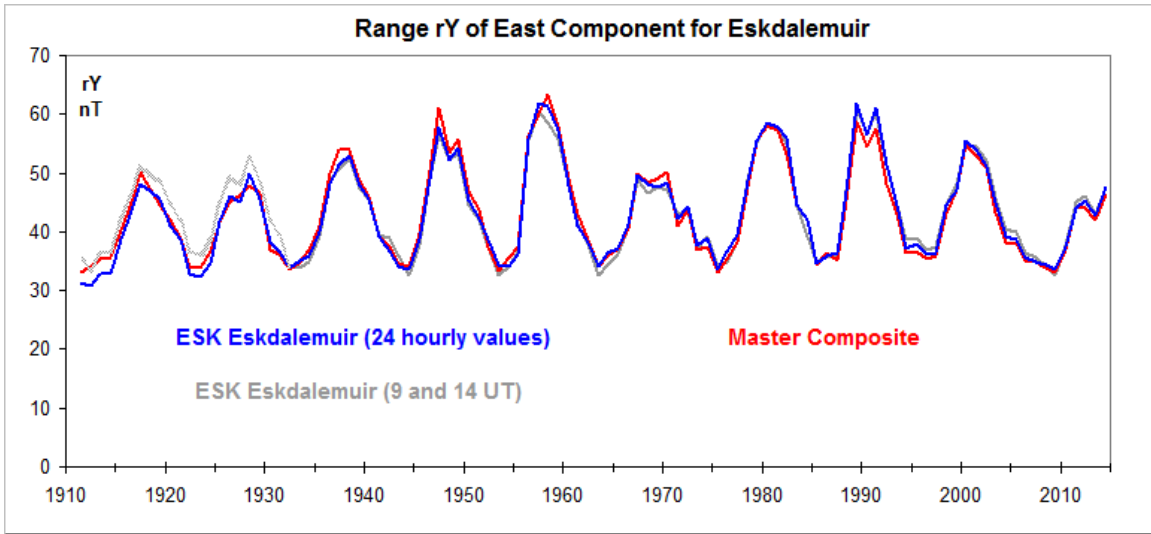
409 decrease of the magnetic effect of the  $S_R$  system over that time, or a 1.3 nT/century  
410 *decrease* that, however, does not seem to be visible in the data at sunspot minima. Other  
411 stations seem to show an *increase* of a similar amount (Macmillan and Droujinina, 2007;  
412 *Yamazaki and Kosch*, 2014) or no increase at all (“Sq(Y) did not increase significantly at  
413 observatories where the main field intensity decreased” (*Takeda*, 2013)). The issue is still  
414 open and several other variables could be in play, such as variation of the upper  
415 atmospheric wind patterns, changes in atmospheric composition, and changes in the  
416 altitude and/or density of the dynamo region (affecting the mix of Hall and Pedersen  
417 conductivities). Our position here shall be not to try to make ad-hoc corrections for the  
418 change of the main field.

419 The Eskdalemuir station (ESK) has been in almost continuous operation with good  
420 coverage since 1911. After getting correct data (MacMillan and Clarke, 2011), the  
421 normalization procedure begins with regression of the Master  $rY$  against the observatory  
422 (ESK in this case), Figure 8. Outliers, if any, are identified and omitted. We find that,  
423 almost always, the regression line goes through the origin within the uncertainty of the  
424 regression, so we force it through the origin (occasionally a better fit is a weak power law  
425 which we then use instead).



438 Figure 8: Linear regression of  $rY$  for the Master against Eskdalemuir (ESK).  
439 On account of significant missing data in 1984, the data point for that year  
440 (red circle) is a clear outlier and has not been included in the regression. The  
441 slope of the regression line indicates the factor by which to multiply the  
442 station value to normalize it to the Master Composite.

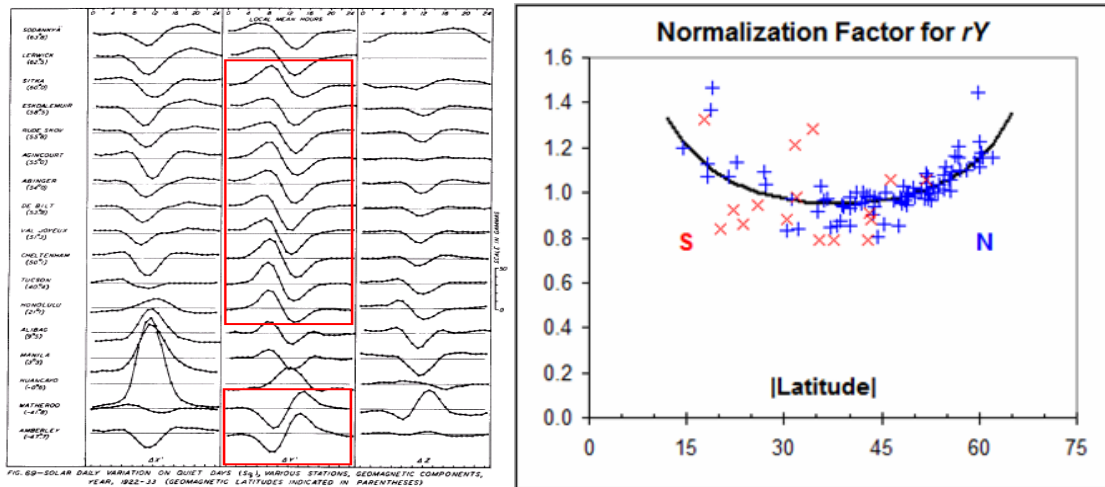
443 When the normalized data is plotted together with the Master Composite (e.g. Figure 9) a  
444 further visual quality control is performed and stations with large discrepancies (mostly  
445 of unknown causes) are omitted from further analysis. Such stations also have an  
446 unsatisfactory Coefficient of Determination for the regression (below  $R^2 = 0.85$ ).



447

448 Figure 9: The unbroken series of  $rY$  ranges of the East-Component for Eskdalemuir  
 449 (ESK, blue) scaled to the Master Composite (red), based on hourly averages 1911–  
 450 2014 using the slope (1.055) from Figure 8. Using only the two values at 9<sup>h</sup> and 14<sup>h</sup>  
 451 local time (happens to be UT) the grey curve results (the scaling factor is 8%  
 452 higher).

453 If hourly averages or hourly spot-values are available, the range is calculated simply as  
 454 the difference between the largest and the smallest hourly values of the yearly average  
 455 curve. Because the curves are much alike (*c.f.* Figure 10) for stations between latitudes  
 456 15° and ~62°, varying mainly in amplitude, only two values at fixed hours during the day  
 457 time are actually needed to determine the daily range, as shown in Figure 9 (the grey  
 458 curve).



459

460 Figure 10: (Left) Diurnal variation of the three geomagnetic components, X, Y  
 461 (middle), and Z, organized according to latitude Red boxes show how the variation  
 462 is very similar for a broad range of latitudes (Vestine et al., 1947). (Right) The  
 463 normalization factor as a function of latitude (blue: Northern Hemisphere, red:  
 464 Southern Hemisphere).

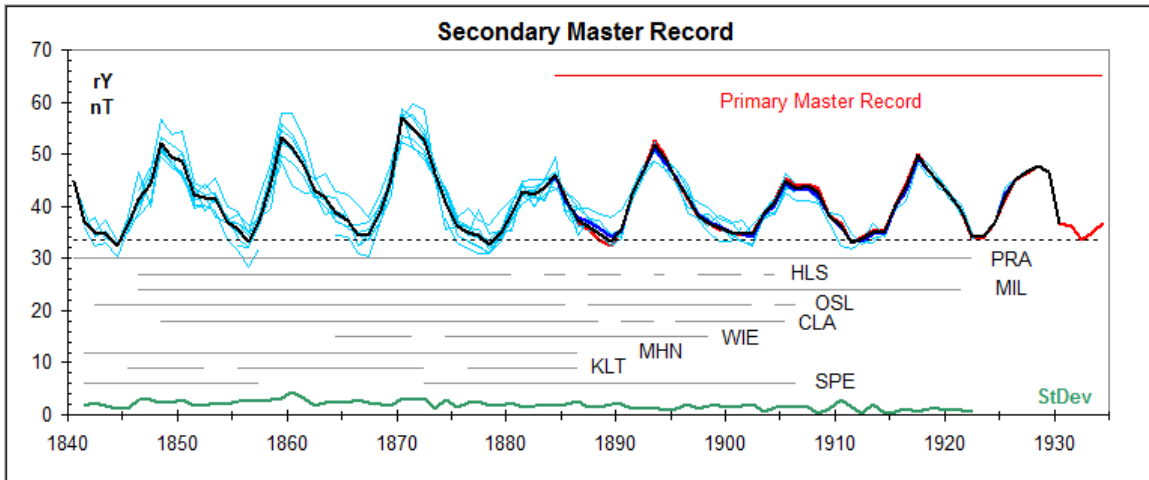
465 Many observatories operating during the 19<sup>th</sup> century were, in fact, only observing a few  
466 times per day. The fit to the Master Composite is nearly as close as for the full 24-hour  
467 coverage, because the two hours chosen are near the average times of maximum effect.  
468 There is small systematic discrepancy for ESK before 1932 due to a change of data  
469 reduction in 1932 (MacMillan and Clarke, 2011). Because such meta-information is  
470 rarely available, we generally make no attempt to correct for known and unknown minor  
471 changes. Large discrepancies or variance cause us simply to reject the data in question.

## 472 **7.1. On ‘Homogeneous’ Data**

473 There is an important, if somewhat philosophical, point to be made here about the  
474 misguided notion (Lockwood *et al.*, 2013) that using only a *single* station at any one time  
475 instead of all available and relevant data is somehow inherently ‘better’ because the  
476 single-station series would be more ‘homogeneous’. This fallacy (leading to erroneous  
477 conclusions, *e.g.* Lockwood *et al.* (1999), Svalgaard *et al.* (2004), Clilverd *et al.* (2005),  
478 and Lockwood *et al.* (2013)) ignores the possibilities of (unreported, unknown, or  
479 disregarded) changes of observing procedure and data handling (MacMillan and Clarke,  
480 2011), of changes of instrumental scale values (Svalgaard, 2014), and of influences of  
481 changing local conditions or aging instruments (Malin, 1996; Lockwood *et al.*, 2013).  
482 The situation is analogous to the clear superiority of the high-quality world-wide *am*  
483 index (Mayaud, 1967), constructed from a carefully calibrated global network of 24  
484 stations, over the limited-quality *aa* index (Mayaud, 1972) constructed from only a single  
485 pair of stations. The *u* measure, if constructed from single-station data at a time  
486 (Lockwood *et al.*, 2013), the *aa* index constructed from a single station-pair at a time,  
487 and the Zürich sunspot number *Rz* constructed from observations largely at a single  
488 station (Waldmeier, 1971) were all optimistically, and somewhat pompously, claimed to  
489 be ‘homogenous’, but turned out not to be so, when re-examined critically and compared  
490 with multi-station or multi-index reconstructions (Svalgaard, 2014; Svalgaard and  
491 Cliver, 2007; Lockwood *et al.*, 2006; Lockwood *et al.*, 2014a; Clette *et al.*, 2014). Claims  
492 of homogeneity can only be made after extensive cross-checking with *other* datasets. We  
493 take the view, which as a bonus also allows an estimate of data uncertainties, that more  
494 data, carefully vetted, is better than less data.

## 495 **7.2. A Secondary Master Record**

496 As the Master Record only goes back to 1884 there is a need for a secondary master  
497 record going further back in order that we can normalize and utilize the earliest data  
498 (there is a vast amount of observational data (Schering, 1889) from the 19<sup>th</sup> century still  
499 awaiting digitization and analysis) that may not have overlapping coverage with the  
500 primary master record. So we continue this, somewhat tedious, section with a description  
501 of the construction of the secondary record. A number of stations (Prague PRA, Helsinki  
502 HLS (Nevanlinna, 2004), Milan MIL, Oslo OSL (Wasserfall, 1948), Colaba CLA,  
503 Vienna WIE, Munich MHN, Clausthal KLT, and St. Petersburg SPE) cover the interval  
504 before 1884 and also overlap with the master record. We can therefore normalize the  
505 records from those stations the usual way to the Master Composite and obtain by  
506 averaging the normalized records the sought after secondary master record, Figure 10,  
507 firmly connecting the two master records. Neither master record show any discernable  
508 trend of the sunspot cycle minimum values (dashed lines in Figures 7 and 11).



509

510 Figure 11: The stations PRA, HLS, MIL, OSL, CLA, WIE, MHN, KLT, and SPE  
 511 have data that overlap with the Master Record (coverage shown by bars labeled  
 512 with the station code) and we can thus normalize their records to the Master  
 513 Composite (red curve). Normalized records for individual stations are shown with  
 514 thin turquoise curves (average curve: blue). The thick black curve shows the final  
 515 average when the overlapping part of the Master Composite is included, forming  
 516 the secondary master record.

517 A source of unwanted variability is that metadata is often lacking as to which days and  
 518 which hours were used to determine the ranges reported: all days, or only quiet days (and  
 519 then which ones), what times of the day (including night hours if they suffered a  
 520 substorm, creating a local extremum), and when, or if, such procedural details changed.  
 521 We assume that the normalization absorbs enough of the effect of such changes that we  
 522 can consider them to be akin to ‘noise’, whose average influence diminishes as the  
 523 number of stations increases.

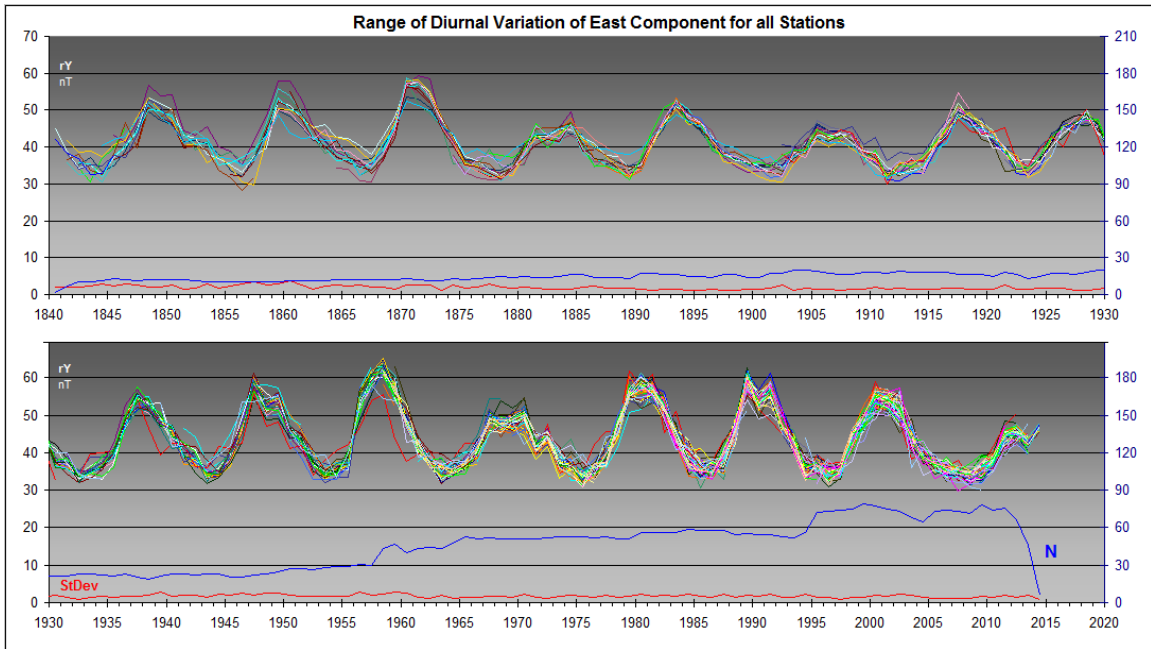
### 524 7.3. The Composite $rY$ Record

525 Normalizing the ranges from the following 129 observatories to the Master Record(s)  
 526 yields the composite shown in Figure 12.

527	AAA	ABG	ABN	AGN	AML	AMS	API	AQU	ARS	ASP	BAL	BDV	BEL
528	BER	BFE	BJI	BMT	BOU	BOX	BSL	CAO	CBI	CDP	CLA	CLF	CLH
529	CNB	COI	CTA	CTO	DBN	DOU	EBR	EKT	ELT	ESA	ESK	EYR	FRD
530	FRN	FUR	GCK	GEN	GLM	GNA	GRW	HAD	HBK	HBT	HER	HLP	HLS
531	HON	HRB	IRT	ISK	JAI	KAK	KDU	KEW	KLT	KNY	KNZ	KSH	LER
532	LNN	LOV	LRM	LVV	LZH	MAB	MBO	MIL	MIZ	MMB	MNH	MNK	MON
533	MZL	NCK	NEW	NGK	NUR	NVS	ODE	OSL	OTT	PAF	PAG	PET	PHI
534	PIL	POT	PRA	PSM	PST	QIX	ROM	RSV	SED	SFS	SIT	SJG	SPE
535	SSH	SVD	TAM	TFS	THJ	THY	TOK	TOO	TOR	TRW	TUC	UPS	VAL
536	VIC	VLJ	VQS	WAT	WHN	WIA	WIE	WIK	WIT	WLH	WNG	YAK	

537 Table 1: IAGA 3-letter codes identifying observing station as listed in *e.g.*  
 538 Rasson (2001) (<http://www.leif.org/research/List-of-IAGA-Stations.pdf>).

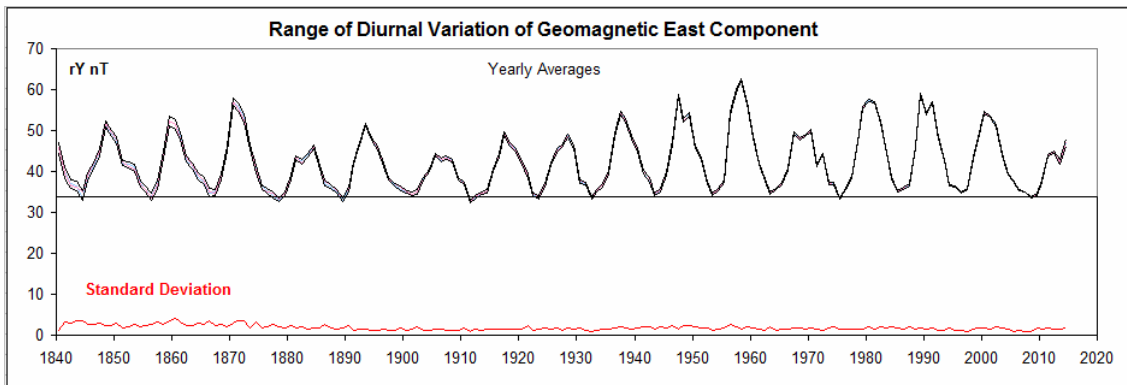




539

540 Figure 12: Normalized yearly average range,  $rY$  in nT, of the geomagnetic East  
 541 component for each of the 129 stations used in the present paper. Different stations  
 542 are plotted with different colors. The standard deviation is shown by the red curve  
 543 at the bottom of each panel and the number of stations,  $N$ , for each station by the  
 544 blue curve.

545 The normalization removes the dependence on latitude and most of the variation due to  
 546 differences in underground conductivity. There remains the (minor) influence of  
 547 geomagnetic activity in the auroral zone and the Ring Current as we did not limit  
 548 ourselves to so-called ‘quiet days’. The multi-colored Figure 12 shows that the ‘spread’  
 549 between stations is rather uniformly about four times the standard deviation,  $SD$ ,  
 550 corresponding to encompassing 95% of the data; this justifies computing the standard  
 551 error  $SE$  of the mean as  $SE = SD/\sqrt{N}$ . Employing this device leads to Figure 13:

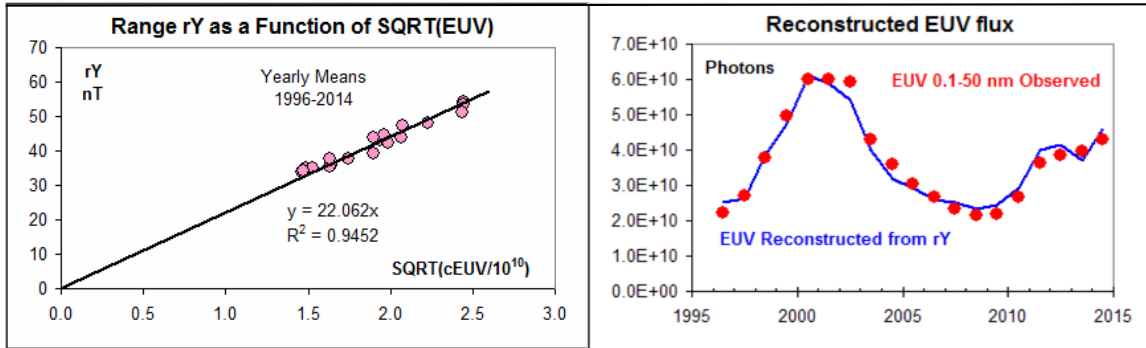


552

553 Figure 13: Normalized yearly average range of the diurnal variation,  $rY$  in nT, of the  
 554 geomagnetic East component. The standard deviation (min 0.90, max 4.23,  
 555 average 1.85 nT) is shown by the red curve at the bottom of the Figure and the  
 556 standard  $\pm 1\text{-}\sigma$  error of the mean surrounds the average (red) curve. The annual  
 557 values of  $rY$  are given in Table 2 at the end of the paper.

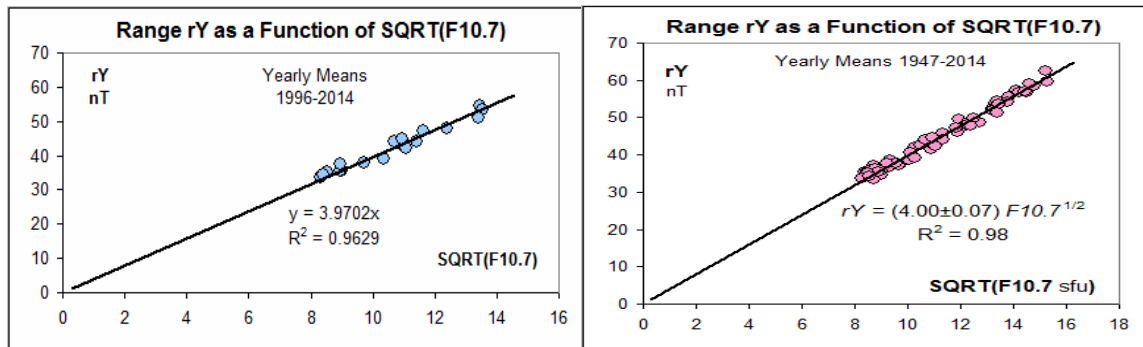
558 **8. Relationship with Solar EUV and F10.7**

559 We can now compare the observed composite range  $rY$  with the theoretical expectation  
 560 that it be proportional to the square root of the EUV flux (and its proxy the F10.7  
 561 microwave flux), Figure 14:



562 Figure 14: (Left) Yearly average ranges  $rY$  plotted against the square root of the  
 563 corrected EUV flux for the years 1996-2014 (see section 3). The offset is  
 564 negligible so there is simple proportionality as expected. (Right) EUV flux  
 565 reconstructed from  $rY$  for 1996-2014 using the slope of the regression line.  
 566

567 The F10.7 microwave flux shows the same square root relationship with  $rY$  as already  
 568 noted by Yamazaki and Kosch (2014). Since measurements of F10.7 go back to 1947 we  
 569 can extend the regression plot that far back as well, Figure 15.  
 570



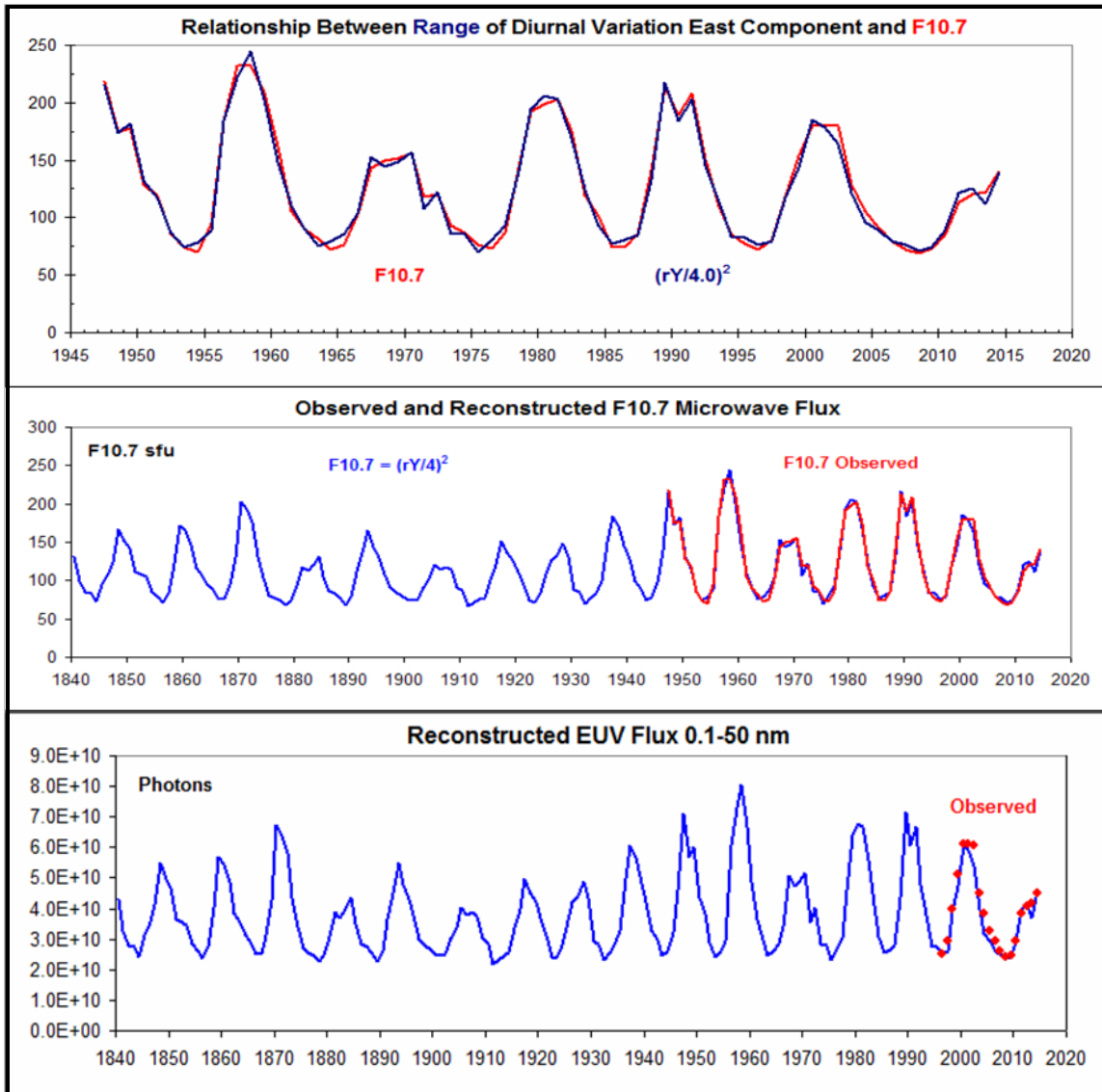
571 Figure 15: (Left) Yearly average ranges  $rY$  plotted against the square root of the  
 572 F10.7 flux for the years 1996-2014 (*c.f.* section 4). The offset is negligible so  
 573 there is simple proportionality as expected. (Right) Extending the regression  
 574 back to the beginning of the F10.7 series in 1947.

575 At this point we have established the calibration factors for  $rY$  to reconstruct the EUV  
 576 and F10.7 fluxes in their respective physical units. The tightness of the correlations and  
 577 the nice homoskedacity (uniform variance) justify using the relationships in reverse and  
 578 calculate the EUV and F10.7 fluxes from  $rY$ :

579 
$$EUV = (rY/22)^2 10^{10} \text{ photons (0.1-50 nm)}$$

580 
$$F10.7 = (rY/4)^2 \text{ sfu}$$

581 Figure 16 shows how successful this procedure is. The reconstruction of F10.7 back to  
 582 1947 is excellent and justifies extending the reconstruction all the back to 1840.



583

584

585

Figure 16: (Top) Yearly average values of the F10.7 flux (blue) compared to the reconstructed values (red) for 1947-2014. (Center) Same, but including the whole period 1840-2014. (Bottom) Yearly average values of the 0.1-50 nm reconstructed EUV flux (blue) and the observed flux (red dots).

586

587

588

589

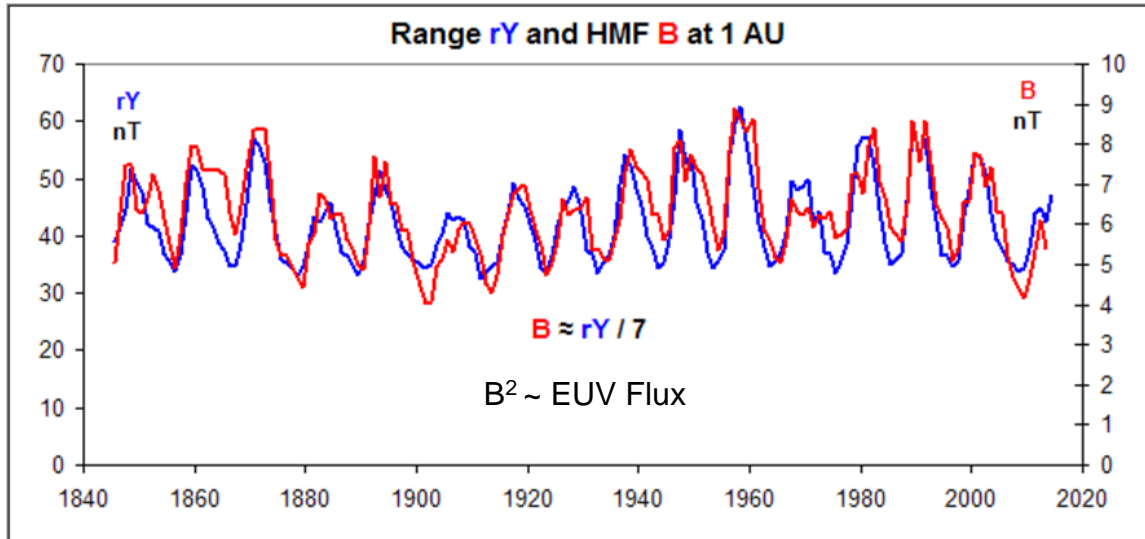
The  $2.5 \cdot 10^{10}$  photons/cm<sup>2</sup>/sec EUV flux in the 0.1-50 nm wavelength range inferred for every sunspot minimum the past 175 years appears to be a ‘basal’ flux, present when visible solar activity has died away. The lack of any variation of this basal flux suggests that the flux (and the network causing it) is always there, presumably also during Grand Minima. If the magnetic network is always present, this means that a chromosphere is also a permanent feature, consistent with the observations of the ‘red flash’ observed during the 1706 solar eclipse (Young, 1881). This is, however, a highly contentious issue (Riley *et al.*, 2015), but one of fundamental importance.

597

As the magnetic field in the solar wind (the Heliosphere) ultimately arises from the magnetic field on the solar surface filtered through the corona, one would expect, at least

598

599 an approximate, relationship between the network field and the Heliospheric field, the  
 600 latter now firmly constrained (Svalgaard, 2015). Figure 17 shows a comparison of the  $rY$   
 601 proxy for the EUV flux from the surface network magnetic field structures, connected in  
 602 the higher solar atmosphere to the coronal magnetic field, and then carried out into the  
 603 Heliosphere to be observed near the Earth.



604  
 605 Figure 17: Yearly average values of the diurnal range  $rY$  of the geomagnetic  
 606 East component (blue, left-hand scale) compared to the inferred magnitude of  
 607 the Heliospheric magnetic field,  $B$ , near the Earth since the 1840s (red,  
 608 right-hand scale).

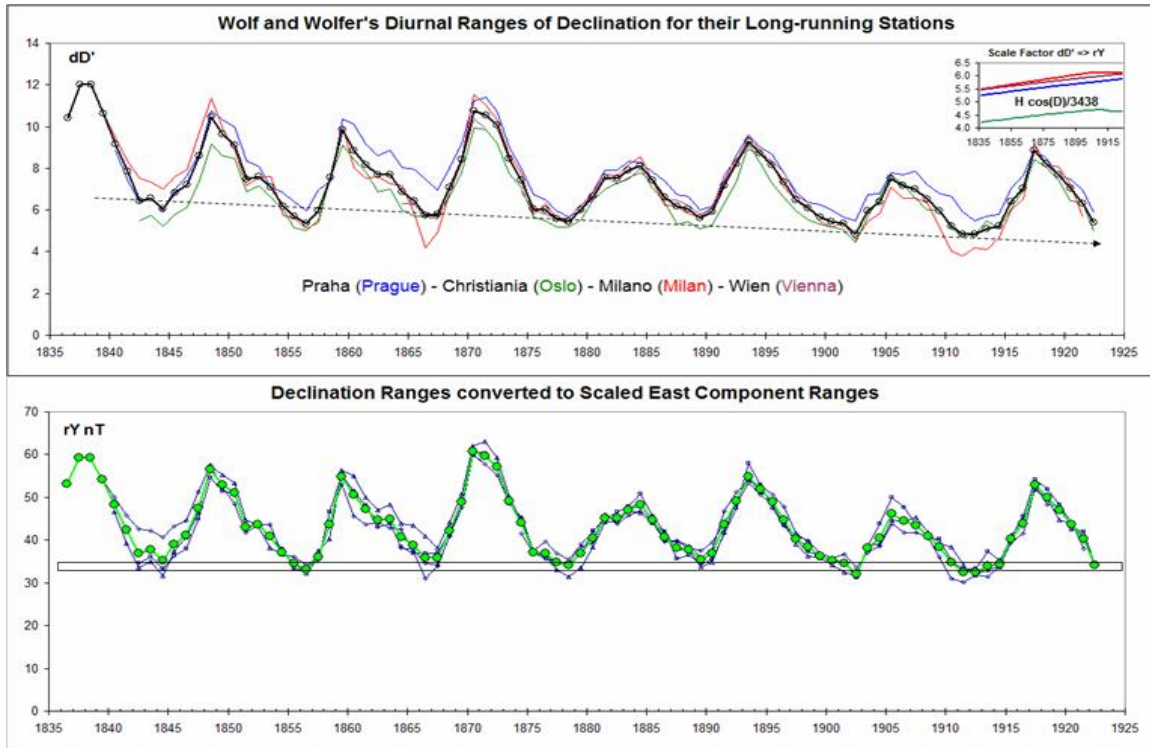
609 Assuming that the EUV flux results from release of stored magnetic energy and therefore  
 610 scales with the energy of the network magnetic field ( $B^2$ ), we can understand the  
 611 correspondence between the Heliospheric field and the network field. Again we are faced  
 612 with the puzzle that there seems to be a ‘floor’ in both and with the question what  
 613 happens to this floor during a Grand Minimum.

## 614 9. A Historical Interlude

615 When Rudolf Wolf discovered the relationship between his Relative Sunspot Number  
 616 and the range of the diurnal variation of the Declination he at once realized that the  
 617 relationship forded an independent check of the sunspot number and proceeded to collect  
 618 and to request variation data from observers at (the often newly established) geomagnetic  
 619 observatories and to compare the observations with his Relative numbers from year to  
 620 year. At times the geomagnetic data would arrive belatedly and Wolf would *predict* from  
 621 his relationship what the range would be and he was generally correct. In 1870 Wolf  
 622 became ‘alarmed’ (Loomis, 1873) because the computed and observed variations  
 623 seriously disagreed and Wolf, being so convinced that the relationship was real and  
 624 physical and should be obeyed, consequently (Wolf, 1872) adjusted his method of  
 625 comparing sunspot observers in order to make the anomaly go away such as to restore the  
 626 agreement between the solar and the terrestrial data. Wolf continued to collect  
 627 geomagnetic data until his death, and his successor, Wolfer, carried on until 1922 when

628 finally the geomagnetic comparisons were discontinued as some participating  
629 observatories were shut down.

630 A factor that perhaps also contributed to the abandonment of the geomagnetic  
631 comparisons was that the relationship appeared to be changing with time such that the  
632 original coefficients were no longer applicable, thus undermining the rationale for  
633 comparing the solar and terrestrial data; the influence of the Sun seemed to be steadily  
634 diminishing, Figure 18 (top panel); and there was general doubt about the validity of the  
635 relationship (Chapman and Bartels, 1940).



636  
637 Figure 18: (Top) Diurnal range,  $dD$ , of Declination reported by Wolf and Wolfer  
638 for the four long-running stations: Prague, Oslo, Milan, and Vienna. The black  
639 curve with circle symbols shows the average of the four stations. The range  
640 shows a clear secular decrease, casting doubt on the physical meaning of the  
641 sunspot-range relationship. The inset shows the secular change of the conversion  
642 factors from  $dD$  to  $rY$  for the four stations, due to the changing main  
643 geomagnetic field. (Bottom) Taking the secular change of the conversion factors  
644 into account removes the secular change of the geomagnetic response,  $rY$ , and  
645 restores the relationship as well as reducing the spread from station to station  
646 (the average is shown by the green curve and symbols). Note, that the values at  
647 each solar minimum are very similar (horizontal bar).

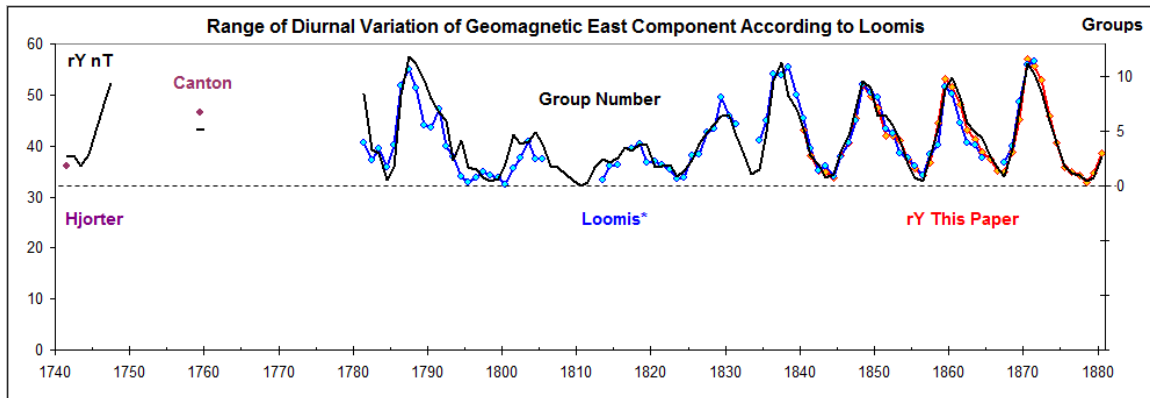
648 Today we know that the relevant parameter for the geomagnetic response is the East  
649 Component,  $Y$ , rather than the Declination,  $D$ . Converting  $D$  to  $Y$  (using  $Y = H \sin(D)$  and  
650  $rY = H \cos(D) dD$ ) restores the stable correlation without any significant long-term drift  
651 of the base values. So Rudolf Wolf was right, after all.  
652

653 **10. Earliest Observations of the Diurnal Range**

654

655 Even before the ‘Magnetic Crusade’ of the 1840s we have scattered observations of the  
656 diurnal variation of the Declination. A detailed discussion of the early data will be the  
657 subject of a separate paper. Here we shall limit ourselves to early data mainly collected  
658 and published by Wolf and reduced by Loomis (1870, 1873) to the common scale of  
659 Prague, Figure 19.

660

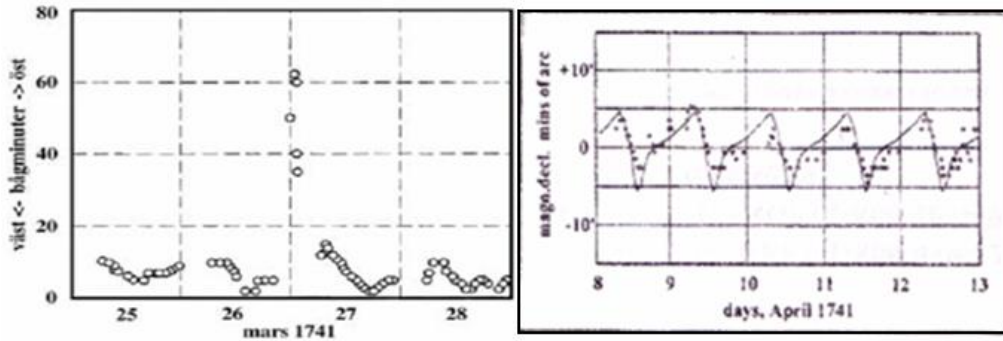


661

662 Figure 19: The range,  $rY$ , of the diurnal variation of the geomagnetic East  
663 component determined from the daily range of Declination (given by Loomis,  
664 1870, 1873) converted to force units in the East direction (blue curve) and then  
665 scaled to match  $rY$  (this paper, red curve), supplemented with observations by  
666 Canton (1759) and Hjorter (1747). The Sunspot Group Number (Svalgaard and  
667 Schatten, 2015) is shown (black curve without symbols) for comparison scaled  
668 (right-hand scale) to match  $rY$ .

669 Loomis drew two important and prescient conclusions: 1) the basal part of the “diurnal  
670 inequality (read: variation), amounting at Prague to six minutes is independent of the  
671 changes in the sun’s surface from year to year”, and 2) “the excess of the diurnal  
672 inequality above six minutes as observed at Prague, is almost exactly proportional to the  
673 amount of spotted surface upon the sun, and may therefore be inferred to be produced by  
674 this disturbance of the sun’s surface, or both disturbances may be ascribed to a common  
675 cause”. It is encouraging that the Sunspot Group Number series seems to agree well with  
676 the diurnal range series, even for the earliest geomagnetic measurements. Loomis’  
677 conclusions are fully supported by our modern data and analyses.

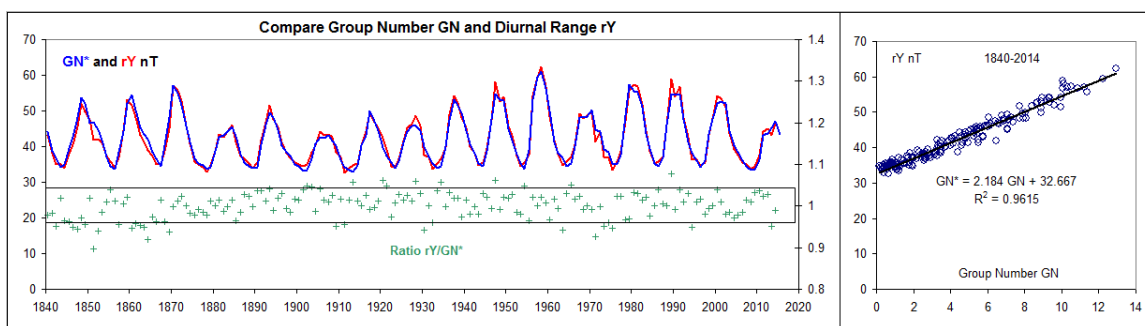
678 Olof Peter Hjorter (with Anders Celsius) made ~10,000 observations of the diurnal  
679 variation of the Declination during 1740-1747 (Hjorter, 1747) at Uppsala, Sweden.  
680 Hjorter’s (and Celsius’) measurements were made with an instrument manufactured by  
681 Graham in London and the data are accurate to about one minute of arc and are the  
682 earliest data of sufficient quality and extent to allow firm determination of the diurnal  
683 variation. The original notebooks with observations have been preserved (and kindly  
684 made available to us by Olof Beckman, Uppsala) and a detailed analysis will be reported  
685 in a separate paper (Svalgaard and Beckman, 2016; a summary to be incorporated in the  
686 present one). At this point we only note that the variation at the sunspot minimum in  
687 1741 was very similar to the variation at nearby Lovö in 1997, Figure 20.



688 Figure 20: (Right) Observations by Olof Hjorter of the variation of the  
 689 Declination at Uppsala during the spring of 1741. The diurnal range was about  
 690 10 arc minutes, comparable to that at nearby Lovö magnetic observatory in  
 691 April 1997 (full drawn curve). The observations (left panel) of the large  
 692 disturbance on March 27 (old style), 1741 were obtained during a great auroral  
 693 display also observed by Graham in London, proving that auroral and magnetic  
 694 phenomena were connected and were not just local effects (Beckman, 2001).  
 695

696 **11. Comparison with the Sunspot Group Series**

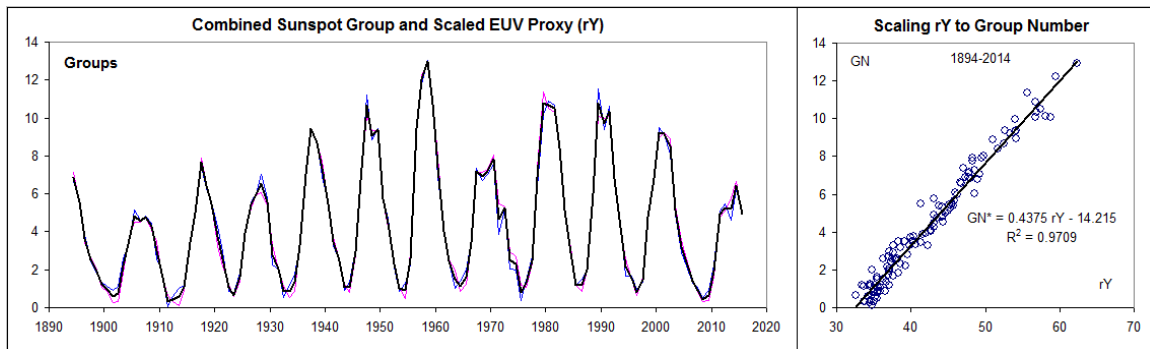
697 Although it is important to stress that the Sunspot Group Number series (Svalgaard and  
 698 Schatten, 2015) is a pure solar index and that the Diurnal Range series (Svalgaard, this  
 699 paper) is a pure terrestrial index, it is also important to compare the two series to check  
 700 for disagreements or differing trends. After all, we are concerned with quantifying  
 701 manifestations of the long-time variation of the same underlying cause, the Sun's  
 702 magnetic field. In order to compare the series we first put them on the same scale by  
 703 regressing  $rY$  against the group number  $GN$ , as shown in the right-hand panel of Figure  
 704 21. Then we can plot the series for easy visual comparison and also take the ratio for a  
 705 numerical measure of the similarity, Figure 21.



706  
 707 Figure 21: The Group Number (blue curve) scaled to match the Diurnal Range  
 708 (red curve) using the regression equation obtained in the right-hand panel. The  
 709 ratio (green symbols) between the two measures is  $1.00 \pm 0.04$  (box).

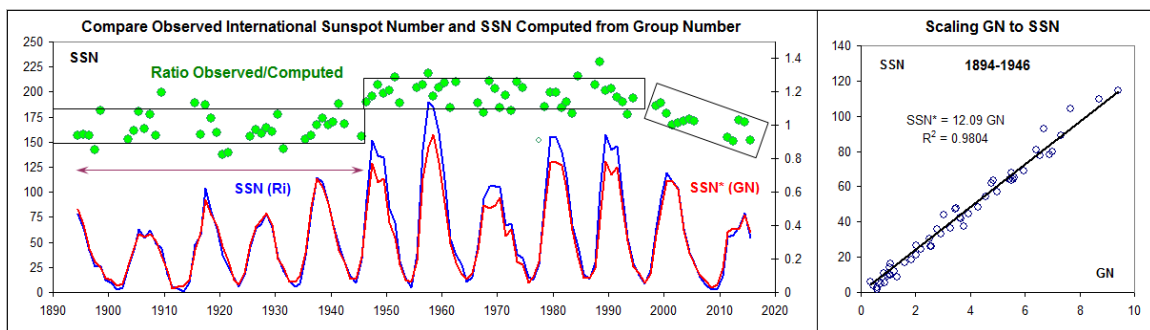
710 The ratio between the diurnal range and the scaled group number is slightly smaller than  
 711 unity during 1840-1870, but is still within the combined error bar for the two series, so  
 712 the geomagnetic data are excellent complements to the direct count of sunspot groups.  
 713 Accepting this, justifies constructing a composite of  $GN$  and  $rY$  in terms of the group

714 count so we can compare with the sunspot number, Figure 22. We consider this  
 715 composite to be a ‘true’ representation of ‘solar activity’, or to alternatively *define* ‘solar  
 716 activity’ because of how closely it correlates with the F10.7 microwave flux.



717  
 718 Figure 22: A composite Group Number (black curve) constructed as the average  
 719 of the observed Group Number,  $GN$ , (pink curve) and the EUV proxy ( $rY$ , blue  
 720 curve) scaled to  $GN$  according to the regression equation shown in the right-  
 721 hand panel. We chose the time after Wolf’s death in 1893 to exclude possible  
 722 contamination or uncertainty from the use of his small telescope (*c.f.* Figure 4 of  
 723 Svalgaard and Schatten (2015)).

724 The first step is to scale the composite Group Number series,  $GN'$ , to the Relative  
 725 Sunspot Number,  $SSN$ . Hoyt and Schatten (1998) found the scaling factor to be given by  
 726  $SSN = 12.08 GN$ . By sheer coincidence we find the scaling factor to be 12.09 (right-hand  
 727 panel of Figure 23) for the time interval 1894-1946. The reason for this choice is that  
 728 there is good evidence that Max Waldmeier (1948) introduced an effective weighting of  
 729 sunspots according to size and complexity in 1947 (section 5.2 of Clette et al. (2014),  
 730 Svalgaard and Cagnotti (2015)). Figure 23 shows the observed  $SSN$  (blue curve) as  
 731 reported by SILSO and the scaled values of  $GN$  (red curve; for convenience we drop the  
 732 prime mark from now on).

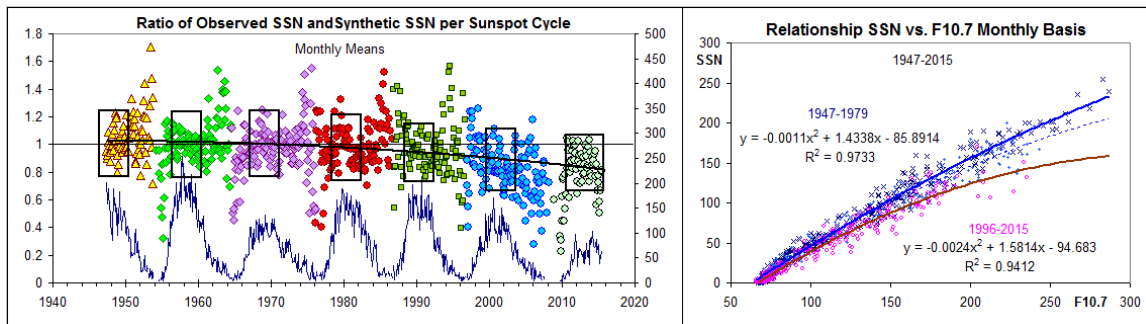


733  
 734 Figure 23: Comparison between the observed International Relative Sunspot  
 735 Number series (blue curve,  $SSN(Ri)$ ) and the composite Group Number series  
 736 scaled (red curve,  $SSN*(GN)$ ) to match  $SSN(Ri)$  during the interval 1894-1946  
 737 (using the regression equation from the right-hand panel). For years where both  
 738 series have values larger than 20 (to avoid the large noise resulting from ratios  
 739 of small numbers) we plot the ratio between them (green dots with right-hand  
 740 scale).



741 The large ‘boxes’ contain 90% of the data points. The average ratio for the box 1894-  
 742 1946 is (not surprisingly) 0.990, but for the 1947-1994 box the average ratio is 1.192,  
 743 which is an increase by a factor 1.204, giving a measure of the inflation of the reported  
 744 SSN from 1947 onwards. This matches the average inflation derived from direct counting  
 745 of spots, with and without weighting (section 5.2 of Clette *et al.* (2014); Svalgaard and  
 746 Cagnotti (2015)).

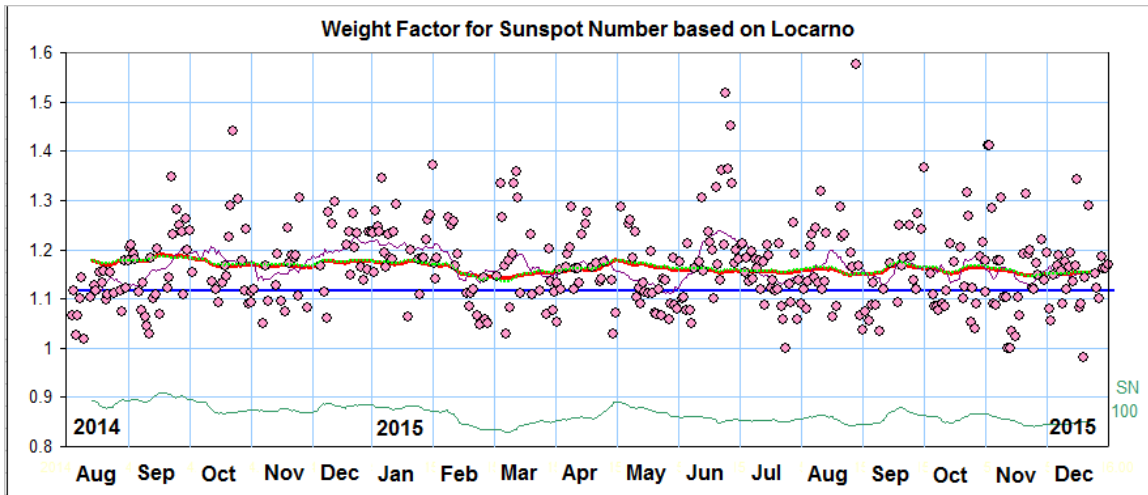
747 What *is* notable, however, is the steady decline of the ratio from at least about 1995 to the  
 748 present time. This discrepancy between the reported SSN and the ‘true’ solar activity (as  
 749 measured by the equivalent F10.7, *rY*, and *GN* indices that all correlate so well with each  
 750 other) has been noted before, *e.g.* by Svalgaard and Hudson (2010) and others. To get a  
 751 better indication of the details of the decline we increase the time resolution from one  
 752 year to one month. At the higher resolution the relationship between the SSN and F10.7 is  
 753 no longer nearly linear. The right-hand panel of Figure 24 shows a 2<sup>nd</sup>-order fit to the  
 754 data during the Zürich-era, assuming that the data are homogenous enough throughout  
 755 that time. We shall use that fit to construct a synthetic SSN to compare with the reported  
 756 SSN, Figure 24.



757

758 Figure 24: Monthly values color-coded per sunspot cycle of the ratio between  
 759 the reported Sunspot Number (itself shown at the bottom of the Figure) and a  
 760 Synthetic Sunspot Number derived from the F10.7 microwave flux using the  
 761 regression equation for the interval 1947-1979 given in the right-hand panel  
 762 (blue curve).

763 The monthly data show the same steady decline of the ratio so we’ll have to accept that  
 764 this is a real effect. What could be the cause of this decline of the Sunspot Number  
 765 compared to F10.7? Has the weighting of sunspots been abandoned since ~1994? No, the  
 766 analysis in Clette *et al.* (2014) shows that it has not. In addition, the observers in Locarno  
 767 since August 2014 report both the weighted count and the un-weighted (actual) count of  
 768 sunspots. Figure 25 shows the observed weight factor computed from their recent reports.



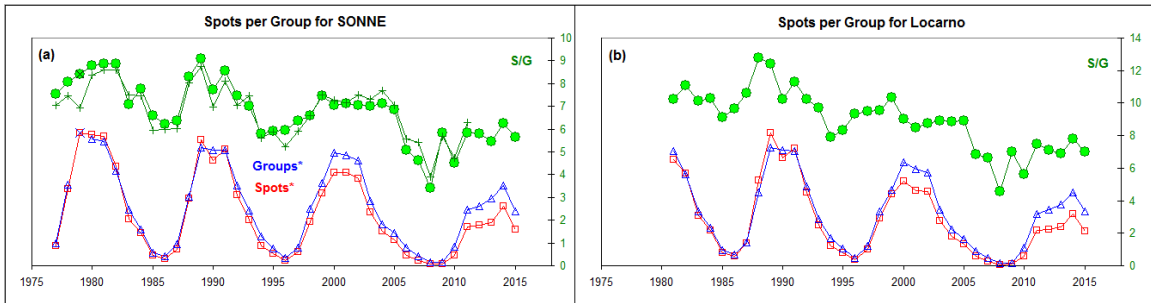
769

770 Figure 25: The ratio of the weighted *SSN* and the un-weighted (real) *SSN*  
 771 reported by Locarno (brown dots) for each daily observation since August,  
 772 2014. The red curve shows the expected 27-day average weight factor computed  
 773 from the formula in Clette *et al.* (2014). The green curve at the bottom of the  
 774 Figure shows the 27-day average sunspot number (version 2). The blue line: see  
 775 text.

776 For this low to medium level of sunspot activity (average *SN* = 81) the average weight  
 777 factor was 1.162, well above the suggested result (1.116, blue line) of the invalid analysis  
 778 by Lockwood *et al.* (2014b), so we have to look elsewhere for an explanation of the  
 779 decline.

### 780 11.1. Number of Spots per Group is Not Constant

781 The basic idea behind the Group Sunspot Number was that the number of spots per group  
 782 is constant. Even in Wolf's definition of the Relative Sunspot Number = 10 Groups +  
 783 Spots that assumption is built-in, as the factor of 10 for the groups is held constant. We  
 784 can investigate the validity of this assumption for recent solar cycles using data from the  
 785 German SONNE network of sunspot observers (Bulling, 2013) and Swiss reference  
 786 station. As we know, to this day the Locarno observers weight larger spots stronger than  
 787 small spots, so the weighted spot count will on average be 30-50% larger than the raw  
 788 count where each spot is counted only once as in Wolf's and Wolfer's original scheme  
 789 (Wolfer, 1907: "Notiert ein Beobachter mit seinem Instrumente an irgend einem Tage *g*  
 790 Fleckengruppen mit insgesamt *f* Einzelflecken, ohne Rücksicht auf deren Grösse, so ist  
 791 die daraus abgeleitete Relativzahl jenes Tages  $r = k(10g+f)$ "). The SONNE observers do  
 792 not employ weighting: each spot is counted only once. It is important that for both groups  
 793 of observers, the counting methods (albeit different) have been unchanged over the  
 794 period of interest.



795

796

797

798

799

800

801

802

803

Figure 26: The number of spots per group as a function of time (green dots) for the ~500,000 individual observations made by the SONNE network (left) and for Locarno (right). The green curve with pluses shows the ratio derived from the raw counts, not normalized with  $k$ -factors, and yet not significantly different. The lower part of the panels shows the variation of number of groups (blue triangles) and of the number of spots (red squares) both scaled to match each other before 1992. Note for both series the decreasing spot count, relative to the group count.

804

805

806

807

808

809

810

811

Figure 26 shows that the average number of spots per group has been decreasing steadily for both SONNE and Locarno and is therefore not due to drifts of calibration or decreasing visual acuity of the primary Locarno observer (Sergio Cortesi). If the ‘missing spots’ were large spots with significant magnetic flux one would expect F10.7 and  $rY$  to decrease as well, contrary to the observed trends (Figures 23-24), so the missing spots must be the smallest spots, as also suggested by Lefèvre and Clette (2011). It appears that this may be a natural explanation for the decline of the Sunspot Number compared to F10.7 and  $rY$ .

812

### 11.2. Comparison with Other UV proxies

813

814

815

816

817

818

819

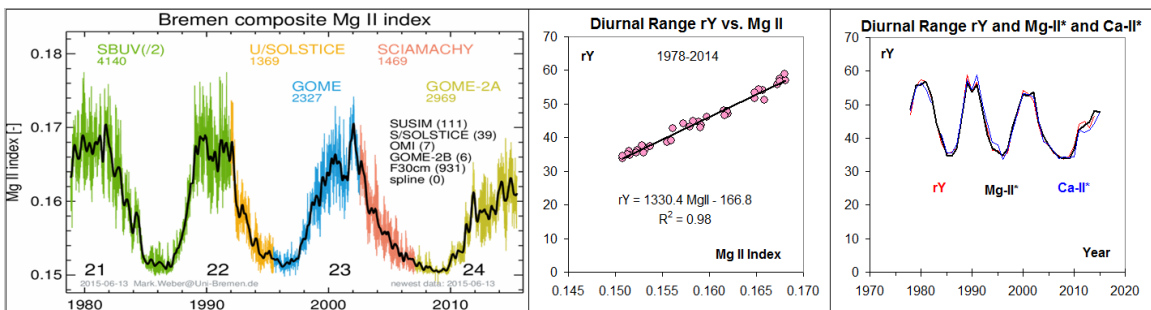
820

821

822

The emission core of the Magnesium II doublet ( $\lambda = 280$  nm) exhibits the largest natural solar irradiance variability above 240 nm. The Mg II doublet is a broad absorption feature with narrow emission peaks in the core. Radiation in the line wings originates in the photosphere and shows much less variability. Therefore, the ratio of line core intensity to wing intensity provides a good estimate of solar variability because the use of an intensity ratio cancels degradation effects. The core-to-wing ratio is frequently used as a proxy for spectral solar irradiance variability from the UV to EUV. The so-called ‘Bremen’ composite series covering 1978-2015 (Snow *et al.*, 2014) utilizes all available satellite data, Figure 27.

823



824 Figure 27: (Left) The Bremen Mg II Index composite (courtesy Mark Weber,  
 825 with permission). (Middle) The yearly averages of the Bremen index have a  
 826 very high correlation ( $R^2 = 0.98$ ) with our  $rY$  composite. (Right) Scaling the Mg  
 827 II index and the (bit more noisy) NSO Ca II K-line index ( $\lambda = 393$  nm) to the  
 828 Diurnal Range,  $rY$ , shows that all three indices agree well over the range from  
 829 EUV to low- $\lambda$  visible.

830 As the Relative Sunspot Number as currently defined deviates from the EUV-UV  
 831 measures it is no longer the usual faithful representation of solar activity. Whether that  
 832 was also the case at times in the past, *e.g.* during Grand Minima, is an open and  
 833 intriguing question. The Group Number, on the other hand, tracks the UV indices closely  
 834 and appears to be a good proxy for solar surface magnetic fields, at least for the past two  
 835 and a half centuries, and again it is not clear what happens during a Grand Minimum.

## 837 12. Conclusions

838  
 839 The Diurnal Range,  $rY$ , of the geomagnetic East component can be determined with  
 840 confidence from observatory data back to 1840 and estimated with reasonable accuracy a  
 841 century further back in time. The range  $rY$  correlates very strongly with the F10.7  
 842 microwave flux and with a range of measures of the EUV-UV flux and thus with the  
 843 solar magnetic field giving rise to these manifestations of solar activity. The variation of  
 844 the range also matches closely that of the Sunspot Group Number and the Heliospheric  
 845 magnetic field, but is at variance with the usual Relative Sunspot Number for the past two  
 846 solar cycles, which we ascribe to a progressive deficit of small sunspots, such that the  
 847 number of spots per group is not constant, but has been steadily decreasing. The range  
 848 (and thus the magnetic activity causing it) reaches a constant (non-zero) floor at every  
 849 solar minimum for which we have data.

850  
 851 Table 2: Yearly values of the Diurnal Range in nT of the Geomagnetic East  
 852 Component with low and high  $1-\sigma$  limits reflecting the standard error of the  
 853 mean. Also listed are the reconstructed values of the F10.7 flux.

Year	Low	Mean	High	F10.7	Year	Low	Mean	High	F10.7
1840.5	42.11	<b>43.15</b>	44.19	116.4	1928.5	48.30	<b>48.61</b>	48.92	147.7
1841.5	37.38	<b>38.05</b>	38.73	90.5	1929.5	45.43	<b>45.76</b>	46.10	130.9
1842.5	34.41	<b>35.04</b>	35.67	76.8	1930.5	37.13	<b>37.60</b>	38.07	88.4
1843.5	34.24	<b>34.96</b>	35.68	76.4	1931.5	36.82	<b>37.13</b>	37.44	86.2
1844.5	33.01	<b>33.85</b>	34.69	71.6	1932.5	33.51	<b>33.71</b>	33.91	71.0
1845.5	37.40	<b>38.01</b>	38.62	90.3	1933.5	34.82	<b>35.14</b>	35.47	77.2
1846.5	39.78	<b>40.50</b>	41.22	102.5	1934.5	36.13	<b>36.52</b>	36.92	83.4
1847.5	44.74	<b>45.40</b>	46.06	128.8	1935.5	39.54	<b>39.86</b>	40.19	99.3
1848.5	51.55	<b>52.07</b>	52.60	169.5	1936.5	48.70	<b>49.04</b>	49.38	150.3
1849.5	48.99	<b>49.83</b>	50.67	155.2	1937.5	53.71	<b>54.13</b>	54.54	183.1
1850.5	46.62	<b>47.55</b>	48.48	141.3	1938.5	52.02	<b>52.48</b>	52.94	172.1
1851.5	41.27	<b>41.92</b>	42.57	109.8	1939.5	47.65	<b>48.25</b>	48.85	145.5
1852.5	41.46	<b>42.05</b>	42.64	110.5	1940.5	44.78	<b>45.17</b>	45.55	127.5
1853.5	40.11	<b>41.10</b>	42.09	105.6	1941.5	39.49	<b>39.94</b>	40.39	99.7

1854.5	36.78	<b>37.34</b>	37.91	87.2		1942.5	37.66	<b>38.11</b>	38.57	90.8
1855.5	34.89	<b>35.69</b>	36.50	79.6		1943.5	34.28	<b>34.61</b>	34.94	74.9
1856.5	33.26	<b>34.11</b>	34.97	72.7		1944.5	35.01	<b>35.50</b>	36.00	78.8
1857.5	35.77	<b>36.79</b>	37.81	84.6		1945.5	39.14	<b>39.57</b>	40.00	97.9
1858.5	43.34	<b>44.40</b>	45.46	123.2		1946.5	46.79	<b>47.40</b>	48.02	140.4
1859.5	51.98	<b>53.14</b>	54.30	176.5		1947.5	57.74	<b>58.15</b>	58.57	211.4
1860.5	50.18	<b>51.46</b>	52.73	165.5		1948.5	52.15	<b>52.67</b>	53.19	173.4
1861.5	47.35	<b>48.21</b>	49.06	145.2		1949.5	53.57	<b>54.07</b>	54.56	182.7
1862.5	42.70	<b>43.13</b>	43.56	116.3		1950.5	45.46	<b>45.83</b>	46.20	131.3
1863.5	40.62	<b>41.25</b>	41.87	106.3		1951.5	42.78	<b>43.14</b>	43.50	116.3
1864.5	38.10	<b>38.84</b>	39.58	94.3		1952.5	37.06	<b>37.42</b>	37.77	87.5
1865.5	36.76	<b>37.47</b>	38.18	87.7		1953.5	34.16	<b>34.48</b>	34.79	74.3
1866.5	34.35	<b>35.10</b>	35.85	77.0		1954.5	35.12	<b>35.42</b>	35.73	78.4
1867.5	34.36	<b>34.92</b>	35.47	76.2		1955.5	37.29	<b>37.62</b>	37.95	88.5
1868.5	38.17	<b>38.71</b>	39.25	93.6		1956.5	53.70	<b>54.21</b>	54.72	183.6
1869.5	44.58	<b>45.11</b>	45.64	127.2		1957.5	59.04	<b>59.43</b>	59.82	220.8
1870.5	56.36	<b>57.06</b>	57.75	203.5		1958.5	61.96	<b>62.29</b>	62.63	242.5
1871.5	54.99	<b>55.73</b>	56.48	194.1		1959.5	56.35	<b>56.77</b>	57.19	201.4
1872.5	52.09	<b>52.88</b>	53.67	174.8		1960.5	47.89	<b>48.29</b>	48.69	145.8
1873.5	45.35	<b>45.81</b>	46.26	131.1		1961.5	41.74	<b>41.96</b>	42.19	110.1
1874.5	40.00	<b>40.70</b>	41.39	103.5		1962.5	37.78	<b>37.95</b>	38.12	90.0
1875.5	35.42	<b>35.88</b>	36.34	80.5		1963.5	34.50	<b>34.79</b>	35.09	75.7
1876.5	34.42	<b>34.96</b>	35.49	76.4		1964.5	35.48	<b>35.66</b>	35.83	79.5
1877.5	33.58	<b>34.30</b>	35.02	73.5		1965.5	36.86	<b>37.05</b>	37.25	85.8
1878.5	32.37	<b>32.88</b>	33.39	67.6		1966.5	40.42	<b>40.61</b>	40.81	103.1
1879.5	34.22	<b>34.71</b>	35.19	75.3		1967.5	48.97	<b>49.23</b>	49.48	151.5
1880.5	38.11	<b>38.58</b>	39.05	93.0		1968.5	47.64	<b>47.87</b>	48.10	143.2
1881.5	42.89	<b>43.35</b>	43.81	117.5		1969.5	48.41	<b>48.61</b>	48.82	147.7
1882.5	42.14	<b>42.54</b>	42.94	113.1		1970.5	49.52	<b>49.83</b>	50.14	155.2
1883.5	43.76	<b>44.18</b>	44.59	122.0		1971.5	41.13	<b>41.32</b>	41.52	106.7
1884.5	45.64	<b>46.02</b>	46.40	132.3		1972.5	44.10	<b>44.24</b>	44.38	122.3
1885.5	40.82	<b>41.32</b>	41.81	106.7		1973.5	36.93	<b>37.16</b>	37.39	86.3
1886.5	36.75	<b>37.38</b>	38.01	87.3		1974.5	36.70	<b>36.97</b>	37.25	85.4
1887.5	36.21	<b>36.62</b>	37.04	83.8		1975.5	33.17	<b>33.41</b>	33.66	69.8
1888.5	34.76	<b>35.17</b>	35.57	77.3		1976.5	35.59	<b>35.81</b>	36.02	80.1
1889.5	33.48	<b>33.95</b>	34.42	72.0		1977.5	38.34	<b>38.61</b>	38.89	93.2
1890.5	35.07	<b>35.43</b>	35.80	78.5		1978.5	46.89	<b>47.10</b>	47.31	138.6
1891.5	41.67	<b>41.94</b>	42.21	109.9		1979.5	55.49	<b>55.73</b>	55.97	194.1
1892.5	46.39	<b>46.72</b>	47.05	136.4		1980.5	57.08	<b>57.38</b>	57.68	205.8
1893.5	51.21	<b>51.59</b>	51.96	166.3		1981.5	56.66	<b>56.88</b>	57.09	202.2
1894.5	47.35	<b>47.73</b>	48.12	142.4		1982.5	51.45	<b>51.74</b>	52.02	167.3
1895.5	45.19	<b>45.50</b>	45.80	129.4		1983.5	44.30	<b>44.55</b>	44.79	124.0
1896.5	41.00	<b>41.38</b>	41.76	107.0		1984.5	38.32	<b>38.62</b>	38.91	93.2
1897.5	37.88	<b>38.15</b>	38.42	91.0		1985.5	35.01	<b>35.25</b>	35.49	77.7
1898.5	36.52	<b>36.82</b>	37.11	84.7		1986.5	35.72	<b>35.92</b>	36.12	80.6
1899.5	35.25	<b>35.59</b>	35.92	79.2		1987.5	36.76	<b>37.06</b>	37.35	85.8
1900.5	34.65	<b>35.03</b>	35.40	76.7		1988.5	45.82	<b>46.02</b>	46.23	132.4
1901.5	34.19	<b>34.56</b>	34.93	74.7		1989.5	58.57	<b>58.85</b>	59.12	216.4
1902.5	34.45	<b>35.03</b>	35.62	76.7		1990.5	53.75	<b>53.98</b>	54.21	182.1

1903.5	38.05	<b>38.34</b>	38.62	91.8		1991.5	56.43	<b>56.74</b>	57.04	201.2
1904.5	40.06	<b>40.39</b>	40.73	102.0		1992.5	47.87	<b>48.07</b>	48.26	144.4
1905.5	43.96	<b>44.31</b>	44.66	122.7		1993.5	42.49	<b>42.68</b>	42.86	113.8
1906.5	42.72	<b>43.08</b>	43.44	116.0		1994.5	36.04	<b>36.33</b>	36.62	82.5
1907.5	43.20	<b>43.49</b>	43.79	118.2		1995.5	36.15	<b>36.31</b>	36.47	82.4
1908.5	42.33	<b>42.70</b>	43.07	114.0		1996.5	34.56	<b>34.73</b>	34.90	75.4
1909.5	38.03	<b>38.36</b>	38.70	92.0		1997.5	35.39	<b>35.51</b>	35.62	78.8
1910.5	36.49	<b>36.99</b>	37.50	85.5		1998.5	42.94	<b>43.11</b>	43.28	116.1
1911.5	32.19	<b>32.56</b>	32.92	66.2		1999.5	47.62	<b>47.80</b>	47.97	142.8
1912.5	33.40	<b>33.82</b>	34.24	71.5		2000.5	54.01	<b>54.22</b>	54.43	183.7
1913.5	34.48	<b>34.84</b>	35.19	75.8		2001.5	53.10	<b>53.29</b>	53.48	177.5
1914.5	34.78	<b>35.15</b>	35.53	77.2		2002.5	50.77	<b>51.06</b>	51.34	162.9
1915.5	39.95	<b>40.30</b>	40.66	101.5		2003.5	43.49	<b>43.74</b>	44.00	119.6
1916.5	43.88	<b>44.30</b>	44.72	122.7		2004.5	38.98	<b>39.17</b>	39.36	95.9
1917.5	49.03	<b>49.50</b>	49.98	153.2		2005.5	37.39	<b>37.52</b>	37.65	88.0
1918.5	46.46	<b>46.85</b>	47.24	137.2		2006.5	35.31	<b>35.45</b>	35.59	78.5
1919.5	44.74	<b>45.14</b>	45.55	127.4		2007.5	34.77	<b>34.90</b>	35.04	76.1
1920.5	41.88	<b>42.24</b>	42.61	111.5		2008.5	33.55	<b>33.68</b>	33.81	70.9
1921.5	38.62	<b>39.26</b>	39.90	96.3		2009.5	34.41	<b>34.60</b>	34.80	74.8
1922.5	34.08	<b>34.47</b>	34.85	74.2		2010.5	37.46	<b>37.62</b>	37.77	88.4
1923.5	33.79	<b>34.18</b>	34.57	73.0		2011.5	43.95	<b>44.16</b>	44.37	121.9
1924.5	36.14	<b>36.63</b>	37.13	83.9		2012.5	44.82	<b>45.01</b>	45.20	126.6
1925.5	41.25	<b>41.67</b>	42.09	108.5		2013.5	42.79	<b>43.08</b>	43.36	116.0
1926.5	44.88	<b>45.28</b>	45.68	128.1		2014.5	46.29	<b>46.69</b>	47.09	136.3
1927.5	45.92	<b>46.19</b>	46.45	133.3		2015.5				129.0

855

856

857

## Acknowledgements

858

We acknowledge the use of data from the following sources: 1) CELIAS/SEM experiment on the Solar Heliospheric Observatory (SOHO) spacecraft, a joint European Space Agency (ESA), United States National Aeronautics and Space Administration (NASA) mission. 2) The Laboratory for Atmospheric and Space Physics (CU) TIMED Mission. 3) The Solar Radio Monitoring Programme at Dominion Radio Astrophysical Observatory operated jointly by National Research Council, Canada and Natural Resources, Canada. 4) The Nobeyama Radio Observatory, NAOJ, Japan. 5) World Data Centers for Geomagnetism in Kyoto and Edinburgh. 6) Data collected at geomagnetic observatories by national institutes according to the high standards of magnetic observatory practice promoted by INTERMAGNET ([www.intermagnet.org](http://www.intermagnet.org)). 7) Data collected by Wolf and Wolfer in *Mittheilungen*. 8) Yearbooks from the British Geological Survey [http://www.geomag.bgs.ac.uk/data\\_service/data/yearbooks/yearbooks.html](http://www.geomag.bgs.ac.uk/data_service/data/yearbooks/yearbooks.html). 9) World Data Center for the production, preservation and dissemination of the international sunspot number <http://sidc.be/silso/>. 10) *Wasserfall* (1948). 11) The SONNE Network <http://sonne.vdsastro.de/index.php?page=gem/res/results.html#provrel>. 12) The Bremen composite Mg II index <http://www.iup.uni-bremen.de/gome/gomemgii.html>. 13) The several World Data Centers for Geomagnetism: <http://www.wdc.bgs.ac.uk/>, <http://wdc.kugi.kyoto-u.ac.jp/hyplt/index.html>, <http://wdciig.res.in/WebUI/Home.aspx>.

874

875

876 We have benefited from comments by Ingrid Cnossen and Ed Cliver. We thank Vladimir  
877 Papitashvili for the CORRGEOM program to compute the geomagnetic field elements for  
878 the years 1590–1995. We thank a referee for insightful comments. This research has  
879 made use of NASA’s Astrophysics Data System. LS thanks Stanford University for  
880 support.

## 881 **References**

- 882 Allen, C.W.: 1948, Critical frequencies, sunspots, and the Sun's ultra-violet radiation,  
883 *Terr. Magn. Atmos. Electr.* **53**(4), 433, doi:10.1029/TE053i004p00433
- 884 Appelton, E.W.: 1947, [http://www.nobelprize.org/nobel\\_prizes/physics/laureates/1947/appleton-](http://www.nobelprize.org/nobel_prizes/physics/laureates/1947/appleton-lecture.pdf)  
885 [lecture.pdf](http://www.nobelprize.org/nobel_prizes/physics/laureates/1947/appleton-lecture.pdf)
- 886 Beckman, O.: 2001, Anders Celsius, *Elementá* **84**, 4
- 887 Bulling, A.: 2013, The SONNE Sunspot Number Network – 35 Years & Counting, *3<sup>rd</sup>*  
888 *SSN Workshop*, <http://www.leif.org/research/SSN/Bulling.pdf>
- 889 Canton, J.: 1759, An Attempt to Account for the Regular Diurnal Variation of the  
890 Horizontal Magnetic Needle; And Also for Its Irregular Variation at the Time of an  
891 Aurora Borealis, *Phil. Trans.* **51**, 398, doi:10.1098/rstl.1759.0040
- 892 Chapman, S., Bartels, J.: 1940, Wolf’s suggested linear relationship, *Geomagnetism* **1**,  
893 224, Oxford, Clarendon Press.
- 894 Chapman, S., Gupta, J.C., Malin, S.R.C.: 1971, The Sunspot Cycle Influence on the Solar  
895 and Lunar Daily Geomagnetic Variations, *Proc. Roy. Soc. Lond.* **324**(1566), 1,  
896 doi:10.1098/rspa.1971.0124
- 897 Chree, C.: 1913, Some Phenomena of Sunspots and of Terrestrial Magnetism at Kew  
898 Observatory, *Phil. Trans. Roy. Soc. Lond. A* **212**, 75, doi: 10.1098/rsta.1913.0003
- 899 Clette, F., Svalgaard, L., Vaquero, J.M., Cliver, E.W.: 2014, Revisiting the Sunspot  
900 Number – A 400–Year Perspective on the Solar Cycle, *Space Sci. Rev.* **186**, 35,  
901 doi:10.1007/s11214-014-0074-2
- 902 Clilverd, M.A., Clark, T.D.G., Clarke, E., Rishbeth, H.: 1998, Increased magnetic storm  
903 activity from 1868 to 1995, *J. Atmos. Solar–Terr. Phys.* **60**, 1047, doi:10.1016/S1364-  
904 6826(98)00049-2
- 905 Clilverd, M.A., Clarke, E., Ulich, T., Linthe, J., Rishbeth, H.: 2005, Reconstructing the  
906 long-term aa index, *J. Geophys. Res.* **110**, A07205, doi:10.1029/2004JA010762
- 907 Cnossen, I., Richmond, A.D., Wiltberger, M.: 2012, The dependence of the coupled  
908 magnetosphere–ionosphere–thermosphere system on the Earth’s magnetic dipole  
909 moment, *J. Geophys. Res.* **117**, A05302, doi:10.1029/2012JA017555
- 910 Didkovsky, L., Wieman, S.: 2014, Ionospheric total electron contents (TECs) as indicators  
911 of solar EUV changes during the last two solar minima, *J. Geophys. Res.* **119**(A), 1,  
912 doi:10.1002/2014JA019977
- 913 Dudok de Wit, T., Bruinsma, S., Shibasaki, K.: 2014, Synoptic radio observations as  
914 proxies for upper atmosphere modelling. *J. Space Weather Space Clim.* **4**, A06,  
915 doi:10.1051/swsc/2014003

916 Emmert, J.T., McDonald, S.E., Drob, D.P., Meier, R.R., Lean, J.L., Picone, J.M.: 2014,  
917 Attribution of interminima changes in the global thermosphere and ionosphere, *J.*  
918 *Geophys. Res.* **119**(A), 6657, doi:10.1002/2013JA019484

919 Fouassier, D., Chulliat, A.: 2009, Extending backwards to 1883 the French magnetic  
920 hourly data series, in *Proceedings of the XIIIth IAGA Workshop on Geomagnetic*  
921 *Observatory Instruments, Data Acquisition, and Processing*, U.S. Geological Survey  
922 Open-File Report 2009–1226, 86, J. J. Love, ed.

923 Gautier, J-A.: 1852, Notice sur quelques recherches récentes, astronomiques et  
924 physiques, relative aux apparences que présente le corps du soleil, *Bibliothèque*  
925 *Universelle de Genève, Archives des sciences physiques et naturelles* **20**, 177, Ferd.  
926 Ramboz et Comp., Genève; <http://tinyurl.com/mgs7hqw>

927 Graham, G.: 1724, An Account of Observations Made of the Variation of the Horizontal  
928 Needle at London, in the Latter Part of the Year 1722, and Beginning of 1723, *Phil.*  
929 *Trans.* **33**, 96, doi:10.1098/rstl.1724.0020

930 Heaviside, O.: 1902, Telegraphy I Theory, *Encyclopedia Britannica* (10<sup>th</sup> ed.) **33**, 213

931 Hjorter, O. P.: 1747, Om Magnet-Nålens åtskillige ändringar etc, *Kong. Svensk. Vet.*  
932 *Handl.* **8**, 27

933 Hoyt, D.V., Schatten, K.H.: 1998, Group sunspot numbers: a new solar activity  
934 reconstruction. *Solar. Phys.* **181**, 491

935 Ieda, A., Oyama, S., Vanhamäki, H., Fujii, R., Nakamizo, A., Amm, O., Hori, T., Takeda,  
936 M., Ueno, G., Yoshikawa, A., Redmon, R.J., Denig, W.F., Kamide, Y., Nishitani, N.:  
937 2014, Approximate forms of daytime ionospheric conductance, *J. Geophys. Res. Space*  
938 *Physics* **119**, 10397, doi:10.1002/2014JA020665

939 Jackson, A., Jonkers, A.R.T., Walker, M.R.: 2000, Four centuries of geomagnetic secular  
940 variation from historical records, *Phil. Trans. Roy. Soc. Lond., A* **358**, 957,  
941 doi:10.1098/rsta.2000.0569. PC-DOS program at  
942 <http://www.leif.org/research/CORRGEOM.EXE>

943 Judge, D.L., McMullin, D.R., Ogawa, H.S., Hovestadt, D., Klecker, B., Hilchenbach, M.,  
944 Möbius, E., Canfield, L.R., Vest, R.E., Watts, R., Tarrío, C., Kühne, M., Wurz, P.: 1998,  
945 First solar EUV irradiances obtained from SOHO by the CELIAS/SEM, *Solar Phys.* **177**,  
946 161, doi:10.1023/A:1004929011427

947 Kennelly, A.E.: 1902, On the Elevation of the Electrically-Conducting Strata of the  
948 Earth's Atmosphere, *Elec. World & Eng.*, **39** 473

949 Koyama, Y., Shinbori, A., Tanaka, Y., Hori, T., Nosé, M., Oimatsu, S.: 2014, An  
950 Interactive Data Language software package to calculate ionospheric conductivity by  
951 using numerical models, *Computer Phys. Comm.* **185**, 3398,  
952 doi:10.1016/j.cpc.2014.08.011

953 Lamont, J.v.: 1851, Ueber die zehnjährige Periode, welche sich in der Größe der  
954 täglichen Bewegung der Magnetnadel darstellt, *Ann. der Physik* **160**(12), 572,  
955 doi:10.1002/andp.18511601206



956 Lean, J.L., Warren, H.P., Mariska, J.T., Bishop, J.: 2003, A new model of solar EUV  
957 irradiance variability, 2, Comparisons with empirical models and observations and  
958 implications for space weather, *J. Geophys. Res.* **108**(A2), 1059,  
959 doi:10.1029/2001JA009238

960 Lean, J.L., Emmert, J.T., Picone, J.M., Meier, R.R.: 2011, Global and regional trends in  
961 ionospheric total electron content, *J. Geophys. Res.* **116**, A00H04,  
962 doi:10.1029/2010JA016378

963 Lefèvre, L., Clette, F.: 2011, A global small sunspot deficit at the base of the index  
964 anomalies of solar cycle 23, *Astr. & Astroph.* **536**, id. L11, 4 pp., doi:10.1051/0004-  
965 6361/201118034

966 Lockwood, M., Stamper, R., Wild, M.N.: 1999, A doubling of the sun's coronal magnetic  
967 field during the last 100 years, *Nature* **399**, 437, doi:10.1038/20867

968 Lockwood, M., Whiter, D., Hancock, B., Henwood, R., Ulich, T., Linthe, H.J., Clarke,  
969 E., Clilverd, M.: 2006, The long-term drift in geomagnetic activity: calibration of the aa  
970 index using data from a variety of magnetometer stations, *Rutherford Appleton*  
971 *Laboratory (RAL) Harwell Oxford, UK*, available at: <http://bit.ly/KjeIio>

972 Lockwood, M., Barnard, L., Nevanlinna, H., Owens, M.J., Harrison, R.G., Rouillard,  
973 A.P., Davis, C.J.: 2013, Reconstruction of geomagnetic activity and near-Earth  
974 interplanetary conditions over the past 167 yr – Part 1: A new geomagnetic data  
975 composite, *Ann. Geophys.* **31**(11), 1957, doi:10.5194/angeo-31-1957-2013

976 Lockwood, M., Nevanlinna, H., Vokhmyanin, M., Ponyavin, D., Sokolov, S., Barnard, L.,  
977 Owens, M.J., Harrison, R.G., Rouillard, A.P., Scott, C.J.: 2014a, Reconstruction of  
978 geomagnetic activity and near-Earth interplanetary conditions over the past 167 yr – Part  
979 3: Improved representation of solar cycle 11, *Ann. Geophys.* **32**(4), 367,  
980 doi:10.5194/angeo-32-367-2014

981 Lockwood, M., Owens, M.J., Barnard, L.: 2014b, Centennial variations in sunspot  
982 number, open solar flux, and streamer belt width: 1. Correction of the sunspot number  
983 record since 1874, *J. Geophys. Res. Space Physics* **119**, 5172,  
984 doi:10.1002/2014JA019970

985 Loomis, E.: 1870, Comparison of the mean daily range of Magnetic Declination, with the  
986 number of Auroras observed each year, and the extent of the black Spots on the surface  
987 of the Sun, *Am. Journ. Sci. Arts, 2<sup>nd</sup> Series* **50**(149), 153

988 Loomis, E.: 1873, Comparison of the mean daily range of the Magnetic Declination and  
989 the number of Auroras observed each year, *Am. Journ. Sci. Arts, 3<sup>rd</sup> Series* **5**(28), 245

990 Love, J.J., Rigler, E.J.: 2014, The magnetic tides of Honolulu, *Geophys. J. Int.* **197**(3),  
991 1335, doi:10.1093/gji/ggu090

992 Maeda, K.: 1977, Conductivity and drift in the ionosphere, *J. Atmos. Terr. Phys.* **39**,  
993 1041, doi:10.1016/0021-9169(77)90013-7

994 MacMillan, S., Droujinina, A.: 2007, Long-term trends in geomagnetic daily variation,  
995 *Earth Planets and Space* **59**, 391, doi:10.1186/BF03352699

- 996 MacMillan, S., Clarke, E.: 2011, Resolving issues concerning Eskdalemuir geomagnetic  
997 hourly values, *Ann. Geophys.* **29**, 283, doi:10.5194/angeo-29-283-2011
- 998 Malin, S.R.C.: 1973, Worldwide Distribution of Geomagnetic Tides, *Phil. Trans. Roy.  
999 Soc. Lond., A* **274**, 551, doi:10.1098/rsta.1973.0076
- 1000 Malin, S.R.C.: 1996, Geomagnetism at the Royal Observatory, Greenwich, *Q. J. Roy.  
1001 Astr. Soc.* **37**, 65
- 1002 Martini, D., Mursula, K., Orispää, M., Linthe, H. –J.: 2015, Long-term decrease in the  
1003 response of midlatitude stations to high-speed solar wind streams in 1914–2000, *J.  
1004 Geophys. Res. Space Physics* **120**, 2662, doi: 10.1002/2014JA020813
- 1005 Mayaud, P.–N.: 1965, Analyse morphologique de la variabilité jour–à–jour de la  
1006 variation journalière “régulière”  $S_R$  du champ magnétique terrestre, II – Le système de  
1007 courants  $CM$  (Régions non–polaires), *Ann. de Géophys.* **21**, 514
- 1008 Mayaud, P. –N.: 1967, Calcul préliminaire d’indices  $K_m$ ,  $K_n$ ,  $K_s$ , ou  $A_m$ ,  $A_n$ , et  $A_s$ ,  
1009 mesures de l’activité magnétique à l’échelle mondiale et dans les hémisphères Nord et  
1010 Sud, *Ann. de Géophys.* **23**(4), 585
- 1011 Mayaud, P.–N.: 1972, The aa indices: A 100-year series characterizing the magnetic  
1012 activity, *J. Geophys. Res.* **77**(34), 6870, doi:10.1029/JA077i034p06870
- 1013 Nevanlinna, H.: 2004, Results of the Helsinki magnetic observatory 1844–1912, *Ann.  
1014 Geophys.* **22**(5), 1691, doi:10.5194/angeo-22-1691-2004
- 1015 Nusinov, A.A. (2006), Ionosphere as a natural detector for investigations of solar EUV  
1016 flux variations, *Adv. Space Res.* **37**(2), 426, doi:10.1016/j.asr.2005.12.001
- 1017 Olsen, N.: 1996, A new tool for determining ionospheric currents from magnetic satellite  
1018 data, *Geophys. Res. Lett.* **23**(24), 3635, doi:10.1029/96GL02896
- 1019 Rasson, J.L.: 2001, The status of the world-wide network of magnetic observatories, their  
1020 location and instrumentation. *Contributions to Geophysics and Geodesy* **31**, 427
- 1021 Richmond, A.D.: 1995, Ionospheric electrodynamics, in *Handbook of Atmospheric  
1022 Electrodynamics* vol. **II**, edited by H. Volland, 249, CRC Press, Boca Raton, FL,  
1023 ISBN:978-0849325205
- 1024 Riley, P., Lionello, R., Linker, J.A., Cliver, E., Balogh, A., Beer, J., Charbonneau, P.,  
1025 Crooker, N., deRosa, M., Lockwood, M., Owens, M., McCracken, K., Usoskin, I.,  
1026 Koutchmy, S.: Inferring the Structure of the Solar Corona and Inner Hemisphere During  
1027 the Maunder Minimum Using Global Thermodynamic Magnetohydrodynamic  
1028 Simulations, *Ap. J.* **802**, 105, doi:10.1088/0004-637X/8-2/2/105
- 1029 Sabine, E.: 1852, On Periodical Laws Discoverable in the Mean Effects of the Larger  
1030 Magnetic Disturbances – No. II, *Phil. Trans. Roy. Soc. Lond.* **142**, 103,  
1031 doi:10.1098/rstl.1852.0009
- 1032 Samson, J.A.R., Gardner, J.L.: 1975, On the Ionization Potential of Molecular Oxygen,  
1033 *Canadian J. Phys.* **53**(19), 1948, doi:10.1139/p75-244

- 1034 Schering, K.: 1889, Die Entwicklung und der gegenwartige Standpunkt der  
 1035 erdmagnetische Forschung, *Geograph. Jahrbuch* **13**, 171,  
 1036 <http://www.leif.org/research/Schering-1889.pdf>
- 1037 Schwabe, S.H.: 1844, Sonnenbeobachtungen im Jahre 1843, *Astron. Nachricht.* **21**(495),  
 1038 233
- 1039 Schuster, A.: 1908, The Diurnal Variation of Terrestrial Magnetism, *Phil. Trans. Roy.*  
 1040 *Soc. London, A* **208**, 163, doi: 10.1098/rsta.1908.0017
- 1041 Shibasaki, K., Ishiguro, M., Enome, S.: 1979, Solar Radio Data Acquisition and  
 1042 Communication System (SORDACS) of Toyokawa Observatory, *Proc. of the Res. Inst. of*  
 1043 *Atmospherics, Nagoya Univ.* **26**, 117
- 1044 Snow, M., Weber, M., Machol, J., Viereck, R., Richard, E.: 2014, Comparison of  
 1045 Magnesium II core-to-wing ratio observations during solar minimum 23/24, *J. Space*  
 1046 *Weather Space Clim.* **4**, A04, doi: 10.1051/swsc/2014001
- 1047 Stewart, B.: 1882, Hypothetical Views Regarding the Connexion between the State of the  
 1048 Sun and Terrestrial Magnetism, *Encyclopedia Britannica (9<sup>th</sup> ed.)* **16**, 181
- 1049 Svalgaard, L., Cliver, E.W.: 2007, Interhourly variability index of geomagnetic activity  
 1050 and its use in deriving the long-term variation of solar wind speed, *J. Geophys. Res.*  
 1051 **112**(A10), doi:10.1029/2007JA012437
- 1052 Svalgaard, L.: 2010, Sixty+ Years of Solar Microwave Flux, *SHINE Conference 2010*,  
 1053 Santa Fe, NM, <http://www.leif.org/research/SHINE-2010-Microwave-Flux.pdf>
- 1054 Svalgaard, L.: 2010, Updating the Historical Sunspot Record, in *SOHO-23:*  
 1055 *Understanding a Peculiar Solar Minimum, ASP Conference Series* **428**, 297, S. R.  
 1056 Cranmer, J. T. Hoeksema, and J. L. Kohl, eds., Astronomical Society of the Pacific, San  
 1057 Francisco, CA, ISBN:978-1-58381-736-0
- 1058 Svalgaard, L.: 2012, How well do we know the sunspot number? in *Comparative*  
 1059 *Magnetic Minima: Characterizing Quiet Times in the Sun and Stars, Proc. IAU*  
 1060 *Symposium* **286**, 27, C. H. Mandrini and D. F. Webb, eds.,  
 1061 doi:10.1017/S1743921312004590
- 1062 Svalgaard, L.: 2014, Correction of errors in scale values for magnetic elements for  
 1063 Helsinki, *Ann. Geophys.* **32**, 633, doi:10.5194/angeo-32-633-2014
- 1064 Svalgaard, L.: 2015, Reconstruction of Heliospheric Magnetic Field 1835-2015, *Solar*  
 1065 *Phys.* (submitted, this issue)
- 1066 Svalgaard, L., Beckman, O.: 2015, Analysis of Hjorter's Observations 1740-1747 of  
 1067 Diurnal Range of Declination, *Solar Phys.* (submitted, this issue)
- 1068 Svalgaard, L., Cagnotti, M.: 2015, The Effect of Weighting of Sunspot Counts, *Solar*  
 1069 *Phys.* (submitted, this issue)
- 1070 Svalgaard, L., Cliver, E.W., Le Sager, P.: 2004, IHV: A new geomagnetic index, *Adv.*  
 1071 *Space Res.* **34**(2), 436
- 1072 Svalgaard, L., Hudson, H.S.: 2010, The Solar Microwave Flux and the Sunspot Number,  
 1073 in *SOHO-23: Understanding a Peculiar Solar Minimum, ASP Conference Series* **428**,

- 1074 325, S. R. Cranmer, J. T. Hoeksema, and J. L. Kohl, eds., Astronomical Society of the  
1075 Pacific, San Francisco, CA, ISBN:978-1-58381-736-0
- 1076 Svalgaard, L., Schatten, K.H.: 2015, Reconstruction of the Sunspot Group Number: the  
1077 Backbone Method, *Solar Phys.* (submitted, this issue)
- 1078 Tapping, K.F.: 1987, Recent solar radio astronomy at centimeter wavelengths: The  
1079 temporal variability of the 10.7-cm flux, *J. Geophys. Res.* **92**(D1), 829,  
1080 doi:10.1029/JD092iD01p00829
- 1081 Tapping, K.F.: 2013, The 10.7 cm solar radio flux ( $F_{10.7}$ ), *Space Weather* **11**, 394,  
1082 doi:10.1002/swe.20064
- 1083 Takeda, M.: 1991, Role of Hall conductivity in the ionospheric dynamo, *J. Geophys. Res.*  
1084 **96**(A6), 9755, doi:10.1029/91JA00667
- 1085 Takeda, M.: 2013, Contribution of wind, conductivity, and geomagnetic main field to the  
1086 variation in the geomagnetic Sq field, *J. Geophys. Res. Space Physics* **118**, 4516,  
1087 doi:10.1002/jgra.50386
- 1088 Waldmeier, M.: 1948, 100 Jahre Sonnenfleckentatistik, *Astron. Mittl. Eidg. Sternw.*  
1089 *Zürich* **16**, No. 152, 1
- 1090 Waldmeier, M.: 1971, An Objective Calibration of the Scale of Sunspot-Numbers,  
1091 *Astron. Mittl. Eidg. Sternw. Zürich* No **304**, 1
- 1092 Wasserfall, K.F.: 1948, Discussion of data for magnetic declination at Oslo, 1843–1930,  
1093 and before 1843, *Terr. Mag. Atmos. Electr.* **53**(3), 279, doi:10.1029/TE053i003p00279
- 1094 Wieman, S.R., Didkovsky, L.V., Judge, D.L.: 2014, Resolving Differences in Absolute  
1095 Irradiance Measurements Between the SOHO/CELIAS/SEM and the SDO/EVE, *Solar Phys.*  
1096 **289**, 2907, doi:10.1007/s11207-014-0519-5
- 1097 Wolf, J.R.: 1852a, Entdeckung des Zusammenhanges zwischen den  
1098 Declinationsvariationen der Magnethadel und den Sonnenflecken, *Mitth. der naturforsch.*  
1099 *Gesell. Bern* 224–264 Nr. **245**, 179
- 1100 Vestine, E. H., LaPorte, L., Lange, I., Scott, W. E.: 1947, The Geomagnetic Field, Its  
1101 Description and Analysis, Carnegie Inst. Of Washington, Publ **580**, Washington D. C.
- 1102 Wolf, J.R.: 1852b, Vergleichung der Sonnenfleckperiode mit der Periode der  
1103 magnetische Variationen, *Mitth. der naturforsch. Gesell. Bern* 224–264 Nr. **255**, 249
- 1104 Wolf, J.R.: 1857, Beitrag zur Geschichte der Entdeckung des Zusammenhanges zwischen  
1105 Erdmagnetismus und Sonnenflecken, *Mitth. über die Sonnenflecken* **III**, 27
- 1106 Wolf, J.R.: 1859, Über die Möglichkeit aus den Sonnenflecken–Relativzahlen die  
1107 erdmagnetische Declinationsvariationen vorauszuberechnen, *Mitth. über die*  
1108 *Sonnenflecken* **IX**, 207
- 1109 Wolf, J.R.: 1872, Beobachtungen der Sonnenflecken im Jahre 1871, sowie Berechnung  
1110 der Relativzahlen und Variationen dieses und Neu-Berechnung derjenigen des  
1111 vorhergehenden Jahres, *Mitth. über die Sonnenflecken* **XXX**, 381
- 1112 Wolfer, A.: 1907, Die Häufigkeit und heliographische Verteilung der Sonnenflecken im  
1113 Jahre 1906, *Astronomische Mitteilungen* **XCVIII**, 252

- 1114 Woods, T.N., Eparvier, F.G., Bailey, S.M., Chamberlin, P.C., Lean, J.L., Rottman, G.J.,  
1115 Solomon, S.C., Tobiska, W.K., Woodraska, D.L.: 2005, The Solar EUV Experiment  
1116 (SEE): Mission overview and first results, *J. Geophys. Res.* **110**, A01312,  
1117 doi:10.1029/2004JA010765
- 1118 Yamazaki, Y., Kosch, M.J.: 2014, Geomagnetic lunar and solar daily variations during  
1119 the last 100 years, *J. Geophys. Res.* **119A**, 1, doi:10.1002/2014JA020203
- 1120 Young, C.A.: 1881, *The Sun*, D. Appleton, New York, 321pp, 182